HHS Public Access

Author manuscript

Sci Transl Med. Author manuscript; available in PMC 2022 March 04.

Published in final edited form as:

Sci Transl Med. 2021 October 13; 13(615): eaba6006. doi:10.1126/scitranslmed.aba6006.

Metabolic regulation by PD-1 signaling promotes long-lived quiescent CD8 T cell memory in mice

Vandana Kalia[1,2,*], **Yevgeniy Yuzefpolskiy**[2], **Adithya Vegaraju**[2], **Hanxi Xiao**[2], **Florian Baumann**[3], **Shashank Jatav**[4], **Candice Church**[5], **Martin Prlic**[6,7,8], **Abhishek Jha**[4], **Paul Nghiem**[5,9], **Stanley Riddell**[9,10], **Surojit Sarkar**[1,2,7,*]

[1]Department of Pediatrics, Division of Hematology and Oncology, University of Washington School of Medicine, Seattle, WA 98195

[2]Ben Towne Center for Childhood Cancer Research, Seattle Children's Research Institute, Seattle WA 98101

[3]QIAGEN Sciences, LLC, 19300 Germantown Rd, Germantown, MD 20874

[4]Elucidata, Cambridge, MA 02139

[5]Department of Medicine, Dermatology Division, University of Washington School of Medicine, Seattle, WA 98195

[6]Vaccine and Infectious Disease Division, Fred Hutchinson Cancer Research Center, Seattle WA 98109

[7]Department of Pathology, University of Washington School of Medicine, Seattle, WA 98195

[8]Department of Global Health, University of Washington School of Medicine, Seattle, WA 98195

[9]Clinical Research Division, Fred Hutchinson Cancer Research Center, Seattle WA 98109

[10]Department of Medicine, University of Washington School of Medicine, Seattle, WA 98195

Abstract

Inhibitory signaling in dysfunctional CD8 T cells through the programmed cell death 1 (PD-1) axis is well established in chronic viral infections and cancers. PD-1 is also transiently induced to high concentrations during priming of acute infections and immunizations, yet its impact on the development of long-lived antigen-independent T cell memory remains unclear. In addition to its expected role in restraining clonal effector expansion, here we show that PD-1 expression on antigen-specific CD8 T cells is required for the development of a durable CD8 T cell memory pool

[*]Corresponding authors sarkarkalia@gmail.com.

Author contributions: YY, HX, AV and FB carried out experiments, analyzed data and prepared figures related to phenotypic and functional assessments of effector and memory cells following infections . YY conducted the metabolic assessments and antibody blockade studies. YY, AV and HX conducted the rapamycin studies. VK and SS conducted the microarray analyses. SJ and AJ performed the metabolomics data analyses. MP provided LM-OVA and OT-1 cells. PN, CC and SR provided critical input on the key aspects of PD-1 expression and blockade in human samples. VK and SS conceptualized the project, designed the experiments, analyzed data, interpreted the results, prepared figures, and wrote the manuscript. All authors assisted with figure or manuscript editing.

Competing Interests: SR is a founder, equity holder, and consultant in Lyell Immunopharma. SR holds patents and licensing royalties with Lyell Immunopharma and Bristol Myers Squibb. SR is a consultant for Adaptive Biotechnologies. AJ and SJ are equity holders in Elucidata Corporation.

after antigen clearance. Loss of T cell-specific PD-1 signaling led to increased contraction and a defect in antigen-independent renewal of memory CD8 T cells in response to homeostatic cytokine signals, thus resulting in attrition of the memory pool over time. Whereas exhausted CD8 T cells regain function after PD-1 checkpoint blockade during chronic viral infection, the pre-existing pool of resting functional bystander memory CD8 T cells established in response to a previously administered immunogen decreased. Metabolically, PD-1 signals were necessary for regulating the critical balance of mTOR-dependent anabolic glycolysis and fatty acid oxidation programs to meet the bioenergetics needs of quiescent CD8 T cell memory. These results define PD-1 as a key metabolic regulator of protective T cell immunity. Further, these results have potential clinical implications for pre-existing CD8 T cell memory during PD-1 checkpoint blockade therapy.

ONE SENTENCE SUMMARY:

PD-1 signals promote development of long-lived quiescent memory CD8 T cells by regulating the balance of glycolysis and fatty acid oxidation.

Introduction

Programmed cell death 1 (PD-1) is one of the central inhibitory receptors during T cell exhaustion in chronic viral infections and cancers (1-4). Induced on T cells following T cell receptor (TCR) stimulation (5, 6), PD-1 expression is sustained at high concentrations on exhausted antigen-specific CD8 T cells during chronic antigen exposure, such as in the context of human immunodeficiency virus (HIV) or hepatitis C virus (HCV) infections and cancers, and curbs T cell responses by attenuating the TCR and costimulatory signaling cascades (2). The functional relevance of PD-1 expression during chronic antigen exposure is evident from the efficient restoration of cytotoxic T lymphocyte (CTL) function and concomitant control of viral loads or tumor burden following antibody blockade of PD-1 signals (7-13). Indeed, PD-1 checkpoint blockade immunotherapy has shown remarkable clinical success in controlling several types of refractory solid tumors, such as renal cell carcinoma, non-small cell lung carcinoma and melanoma (14-21). These findings have led to advances in understanding of the cellular (22, 23) and molecular mechanisms (24-30) underlying PD-1-mediated rescue of exhausted CD8 T cells. Nonetheless, our understanding of how PD-1 signaling regulates the development and maintenance of functional CD8 T cell immunologic memory remains incomplete. This knowledge bears clinical relevance in the context of PD-1 checkpoint blockade immunotherapy, now approved by the US Food and Drug Administration (FDA), for use in multiple solid tumors (31).

Memory CD8 T cells, with canonical properties of antigen-independent homeostatic maintenance, polyfunctionality, and robust responsiveness to secondary challenge, are typically generated in settings of acute infections and immunizations where antigen is controlled in a timely fashion. Although rest from antigenic stimulation is critical for progressive acquisition of quiescent memory properties, CD8 T cell memory fate is defined during early stages of T cell activation and effector differentiation, and is programmed by a multitude of factors including cytokines, costimulatory and coinhibitory signals, and interaction with other immune cells (32-38). PD-1 expression is upregulated on CD8 T cells during acute infections by TCR signals during priming and activation (39), similar

to chronic infections (12). In vitro stimulation of human T cells through the TCR also leads to upregulation of PD-1 (40, 41). This seemingly paradoxical upregulation of an inhibitory receptor during T cell activation is proposed to curb effector responses and associated immunopathology (42) in chronic (43) and acute infections (such as lymphocytic choriomeningitis virus [$LCMV_{Arm}$] (39), rabies and respiratory syncytial virus [RSV] (44-46)). Loss of PD-1 inhibition through germline gene ablation of *pdcd1, pdl1/l2*, or system-wide PD-1/programmed death ligand 1(PD-L1) antibody blockade strategies has been shown to augment effector T cell responses in certain cases, such as LCMV and rabies (12, 39, 44-48), but not others, such as *Listeria monocytogenes* (LM) (49-51). Limited studies have suggested CD8 T cell memory perturbations upon loss of PD-1 inhibition, with contradictory observations of increased (39, 52) memory-fated cells at early time-points, or decreased memory in respiratory infections (48). Hence, further studies are necessary to determine whether early expression of PD-1 during activation has a bearing on CD8 T cell effector and memory fate, whether PD-1 functions in a CD8 T cell-specific manner, or through its effects on other immune cells (32, 33, 36, 53-55), and how PD-1 regulates memory development and maintenance.

In this study we engaged an intersection of phenotypic, functional, metabolomic and transcriptomic analysis centered around the PD-1 pathway, to investigate the CD8 T cell-intrinsic role of PD-1 in promoting the long-lived homeostatic memory pool. Notably, we conducted the studies in a co-transfer setting, where all environmental factors are identical for wild-type (WT) and PD-1 knockout (KO) antigen-specific cells, thus bypassing confounding variables such as clonal competition, altered viral loads, or indirect effects through inhibition of PD-1 signaling on other immune cells. These studies will have implications for immunizations, where CD8 T cell memory outcome may be controlled through manipulation of PD-1, and even in the clinically relevant setting of PD-1 checkpoint blockade immunotherapy of cancers and chronic infections, where bystander memory might be impacted.

Results

Early activation, proliferation, and effector differentiation of CD8 T cells during priming is largely independent of PD-1 signals.

PD-1 is upregulated on antigen-specific CD8 T cells early after TCR stimulation, and is then maintained persistently high during chronic infections, but is markedly downregulated by the peak of effector CD8 T cells responses during acute infections (7, 56). Loss of PD-1 inhibition is associated with increased effector responses and tissue pathology at the peak of effector CD8 T cell expansion in most viral infections (12, 39, 43-48). However, it remains to be defined whether the transient induction of PD-1 expression during CD8 T cell activation in acute infection is associated with early dampening of effector differentiation. To address this, we first confirmed early induction of PD-1 expression in acute and chronic LCMV infection during T cell priming. Expectedly, H-$2D^b$:GP33-specific P14 CD8 T cells induced PD-1 to equally high abundance by days 2 to 3 after infection with either the clone-13 strain (the classic model of antigen persistence, T cell exhaustion, and PD-1 checkpoint blockade), or the three amino acid variant Armstrong strain (57), which causes

an acute infection and results in the formation of durable protective CTL immunity after pathogen clearance (Fig. 1A). Notably, early PD-1 upregulation was observed universally in Listeria monocytogenes (LM) and vaccinia virus (VACV) infections as well (fig. S1A and B), and occurred independently of the number of rounds of cell division (fig. S1C). Consistent with their activated effector status, PD-1^{hi} cells concurrently expressed high concentrations of signature T cell activation markers such as CD25 and CD69 (fig. S1A, B, and D), and displayed archetypal effector molecule expression pattern, such as induction of granzyme B and interferon (IFN)-γ(fig. S1A, B, E, and F). PD-1^{hi} cells also exhibited downregulation of CD62L and CD127 (fig. S1A, B, and E). However, with progression of infection, PD-1 expression on T cells diverged between acute and chronic infections as noted previously (58). PD-1 was maintained at high abundance during chronic antigen (Fig. 1A) and was associated with impaired cytokine production at day 40 (fig. S1F). In contrast, antigen clearance in acute infection was associated with lowered PD-1 expression and maintenance of robust cytokine production in response to antigenic re-encounter (Fig. 1A, fig. S1F). It is important to note that functionally potent resting memory CD8 T cells maintain intermediate PD-1 expression (PD-1^{int}), at an abundance two-folds higher than PD-1^{lo} naïve CD8 T cells, as shown by both protein (Fig. 1A) and transcript concentrations (fig. S1G). This has also been reported in the context of human memory CD8 T cells (59, 60).

Next, we directly investigated whether this transient PD-1 upregulation on CD8 T cells during acute LCMV infection alters early antigen-specific effector responses. For this, we adoptively co-transferred equal precursor frequencies of wild-type (WT) and PD-1 knockout H-2D^{b}:GP33-specific P14 CD8 T cells into same naive C57BL/6 recipients (Fig. 1B). This strategy bypasses any autoimmune defects and alterations of natural killer cells (NK), dendritic cells (DC), macrophages, conventional CD4 T cells, and regulatory T cells typically observed in PD-1-deficient mice and permits a head-to-head comparison of PD-1-deficient P14 cells that were primed, expanded, and differentiated in the same infected milieu as their WT counterparts, including similar viral loads, inflammation, and other immune signals. As suggested by robust activation and effector status during early stages of T cell responses when PD-1 is strongly upregulated, we found that T cell-specific PD-1 ablation exerted minimal impact on early CD8 T cell activation, expansion and effector differentiation at day 2 to 3 after acute viral infection. Both WT and PD-1 ablated subsets proliferated similarly as indicated by the extent of carboxyfluorescein succinimidyl ester (CFSE) dilution (Fig. 1C), and accumulated to largely similar numbers in all lymphoid (spleen, inguinal lymph nodes) and nonlymphoid (lung, liver) tissues analyzed (Fig. 1D); both populations of CD8 T cells upregulated the expression of activation markers CD25 and CD69 (albeit PD-1 ablated cells showed modestly lower CD25 expression); and also expressed stereotypical effector molecules to similar degrees; these included granzyme B, which was quantified directly after cell isolation, and IFN-γ and tumor necrosis factor (TNF)-α, which were quantified in response to antigenic restimulation in vitro (Fig. 1E). These data demonstrate that during early stages of infection and activation, when PD-1 expression is strongly induced on antigen-specific CD8 T cells, targeted ablation of PD-1 in a subset of antigen-specific CD8 T cells minimally impacts activation, proliferation, and effector differentiation.

PD-1 exerts modest regulation of peak effector CD8 T cell responses during acute infection.

Ubiquitous loss of PD-1-mediated inhibition in all immune cells, as occurs in germline deletion or antibody blockade models, is associated with augmented effector T cell responses in distinct viral infections (12, 39, 44-47), but not bacterial infection (49-51). A recent study (48) reported increased effector T cell responses in the lung following loss of PD-1 during localized respiratory infections. To investigate the T cell-specific role of PD-1 in regulating effector responses in lymphoid and nonlymphoid compartments, we compared the function and numbers of WT and PD-1 ablated H-2D^{b}:GP33-specific P14 cells following adoptive co-transfer into WT mice with intraperitoneal LCMV infection, not focalized to the lung. Compared to chronic LCMV$_{Cl\text{-}13}$ infection, where CD8 T cell-specific ablation of PD-1 led to an evident increase in proliferation and accumulation of P14 cells at day 8 after infection (fig. S2A)(12, 47, 48), PD-1 deficient antigen-specific CD8 T cells expanded to largely similar levels as WT cells irrespective of the precursor frequencies [low (2,000 cells) (fig. S2B) or high (100,000 cells) (Fig. 2A, fig. S2B)] as well as single or co-transfer modalities (fig. S2B). Nonetheless, consistent with previous reports (39, 48), PD-1-deficient CD8 T cells exhibited a modest (1.5 to 2 fold) increase in numbers during acute LCMV$_{Arm}$ infection in almost all lymphoid and nonlymphoid tissues analyzed with significant differences noted in lymph node (P<0.05) (Fig. 2A).

With respect to effector differentiation, both WT and PD-1-ablated subsets exhibited similar effector phenotypic characteristics, such as CD62L and B cell lymphoma-2 (Bcl-2) downregulation and induction of granzyme B, T-box expressed in T cells transcription factor (T-bet), and effector state-specific 1B11 glycosylation of CD43 (Fig. 2B). WT and PD-1-deficient effector cells also showed similar production of the effector cytokines, IFN-γ and TNF-α (Fig. 2C), and degranulated to similar extent in response to antigenic restimulation as measured by CD107a/b surface abundance (Fig. 2D). Likewise, the relative proportions (fig. S2C) and absolute numbers (Fig. 2E) of short-lived effector cells (SLEC) and memory precursor effector cell (MPEC) subsets, as distinguished by cell surface markers CD127 and killer cell lectin like receptor G1 (KLRG-1) (34, 35, 37, 61, 62) were similar between WT and PD-1 ablated donor cells in all tissues analyzed.

Importantly, PD-1 competent and deficient effectors were strikingly similar in their global gene expression patterns (Fig. 2F, fig. S2D). Gene set enrichment analysis (GSEA) of canonical effector (Fig. 2G) or memory precursor (Fig. 2H, fig. S2E) signatures failed to distinguish any enrichment in PD-1-competent or deficient effector cells. Likewise, glycolysis and interleukin (IL)-2/signal transducer and activator of transcription 5 (STAT-5) signaling gene signatures, typically associated with effector differentiation (32, 34, 63-65), were also expressed similarly in WT and PD-1-deficient effector cells (fig. S2F and G). To further scrutinize any finer differences between WT and PD-1-deficient effectors that could bear possible biological relevance, we compared row normalized data. As opposed to global normalization of data, which is based on expression of all gene analytes, in row normalization, a given gene is normalized across samples to highlight even minor 1.1-fold differences (fig. S2H). Focusing on a select subset of 36 genes well-established for their increased expression in effector T cells (fig. S2I), row normalization analyses showed

that genes encoding canonical effector molecules, such as perforin and granzymes, cell proliferation regulators, such as cyclin dependent kinase (CDK) and aurora kinase (AURK), or transcription factors, such as T-bet and Blimp-1, and Basic Leucine Zipper ATF-Like Transcription Factor (BATF), associated with effector differentiation, were expressed at largely similar abundance in PD-1-deficient cells (fig. S2H). Collectively, these data demonstrate that, although prolonged upregulation of PD-1 in response to chronic antigen and in lung infections strongly downregulates T cell responses, transient upregulation of PD-1 expression during priming of acute infection exerts few regulatory effects on primary CD8 T cell expansion and effector differentiation.

CD8 T cell-specific PD-1 signals are critical for the development of long-term memory.

We next analyzed the differentiation of PD-1 sufficient and deficient donors into memory phase using the same experimental setting of adoptive cotransfer into naïve mice prior to acute LCMV infection as in Fig. 1B. Long-term follow-up of WT and PD-1 ablated CD8 T cells revealed that, despite similar amounts of memory precursors in both subsets (Fig. 2E), PD-1-deficient effector CD8 T cells numbers were significantly reduced during contraction ($P<0.05$) and CD8 T cell memory maintenance ($P<0.05$) phases (Fig. 3A and B), thus resulting in about 100-fold lower final memory numbers in both lymphoid and non-lymphoid compartments (Fig. 3A, fig. S3A). Reduced numbers of PD-1-deficient CD8 T cells at memory were noted in settings of low (2,000) as well as high (50,000) precursor frequencies (fig. S3B and C), which indicates that these results are not due to intraclonal competition. Likewise, PD-1 deficient GP33, NP396, and GP276 epitope-specificities also showed increased contraction (fig. S3D). Increased contraction of WT $H2D^b$ donor cells in PD-1-deficient recipients compared to WT recipients suggest that, in addition to regulating contraction in a CD8 T cell intrinsic manner, PD-1 may exert CD8 T cell-extrinsic effects as well (fig. S3D). A similar pattern of increased contraction of PD-1-deficient CD8 T cells was also observed during LM and VACV infections (fig. S3E). These findings are consistent with previous reports evaluating respiratory infections (48), with distinct toll-like receptors (TLR), NOD-like receptors (NLR), antigen, cytokine and costimulatory signals (5, 52). Consistent with increased contraction, PD-1-deficient effector cells exhibited significant enrichment of apoptosis gene signature at day 8 ($P<0.001$, Fig. 3C, fig. S3F). Together, with parallel enrichment of IFN-γ response and TNF-α signaling gene signatures in PD-1-deficient effector cells (fig. S3G to J), these observations suggest that inhibitory PD-1 signals might program contraction outcomes during the expansion phase through inhibition of pro-apoptotic pathways downstream of IFN-γ and TNF-α signaling in activated effector T cells (66-68).

We next characterized the phenotypic properties of PD-1 deficient and sufficient memory CD8 T cells. The increased death of PD-1-deficient donors during contraction was followed by largely similar proportions of memory-fated $CD127^{Hi}KLRG\text{-}1^{Lo}$ cells in most tissues analyzed at day 60 (Fig. 3D). However, we noted impaired upregulation of the lymphoid homing molecule, CD62L in PD-1-deficient memory CD8 T cells, with statistically significant differences in spleen ($P<0.05$) and liver ($P<0.05$) observed by day 30 after infection, and in lymph nodes ($P<0.05$) at day 60 (Fig. 3E). Amongst the few PD-1-deficient memory CD8 T cells that remained at memory (day 60 after infection) after >10-fold

decline, both central memory (T_{CM}, $CD127^{Hi}KLRG\text{-}1^{Lo}CD62L^{Hi}$) and effector memory phenotype (T_{EM}, $CD127^{Hi}KLRG\text{-}1^{Hi}CD62L^{Lo}$) cells were similarly reduced by 10-20 fold in all lymphoid and non-lymphoid compartments compared to WT memory CD8 T cells (fig. S3K), thus supporting a generalized overall decline in memory in the absence of T cell-specific PD-1 signals.

We next compared the functional properties of WT and PD-1 ablated memory CD8 T cells. Consistent with similar loss of lymphoid and nonlymphoid memory subsets in the absence of PD-1, we did not observe skewing of memory function (Fig 3F and G, fig. S3L to N). PD-1-deficient memory CD8 T cells fared similarly in function to their WT counterparts when assessed for key functional properties, such as the ability to coproduce IFN-γ and TNF-α in response to antigen stimulation (Fig. 3F, fig. S3L), and recall expansion in response to antigenic rechallenge (Fig. 3G, fig. S3M and N). Purified WT and PD-1 knockout memory CD8 T cells mounted similar expansion in a minimalistic in vitro peptide antigen restimulation assay as determined by CFSE dilution and BrdU incorporation (fig. S3M), and also in the physiologically relevant in vivo setting of heterologous LM-GP33 rechallenge (Fig. 3G, fig. S3N). Similar secondary expansion in response to antigenic restimulation was associated with comparable TCR transduction in PD-1 sufficient and deficient cells, as indicated by similar phosphorylation of S6 in response to cognate antigen (fig. S3O). A longitudinal in vivo follow-up of the secondary responses revealed that PD-1-deficient effector cells underwent more pronounced contraction and contributed less to the secondary memory pool on a per cell basis after antigen clearance (Fig. 3G and fig. S3N), as in the case of primary responses. Together, these data establish a requirement for PD-1 signals in the development of acute infection-induced long-term CD8 T cell memory.

PD-1 signals are necessary for antigen-independent homeostatic maintenance of long-lived memory CD8 T cells.

Increased death of PD-1-deficient CD8 T cells after antigen clearance during the contraction and memory phases suggested a dysregulation in antigen-independent mechanisms of homeostatic maintenance. Contrary to persistent infections, where long-term maintenance of exhausted CD8 T cells is dependent on chronic antigenic stimulation (12, 69, 70), the longevity of canonical memory CD8 T cells is independent of cognate antigen and is largely driven by survival and slow homeostatic turnover in response to common γ-chain cytokines such as IL-7 and IL-15 (71, 72). Hence, we first compared the abundance of common γ-chain cytokine receptors on WT and PD-1-deficient cells. PD-1 sufficient and deficient donors similarly expressed IL-7Rα, CD132 (the common γ-chain signaling chain) and CD122 (the common β-chain signaling chain) during memory homeostasis (Fig. 4A). Consistent with similar expression of cytokine receptor expression, the PD-1-deficient memory CD8 T cells exhibited similar intracellular transduction of the homeostatic cytokine signals through the Janus Kinase (JAK)-STAT pathway, as shown by similar STAT5 phosphorylation directly after isolation or after in vitro stimulation with IL-7 and IL-15 at increasing concentrations (Fig. 4B, fig. S4A).

Despite similar common γ-chain cytokine receptor expression and downstream STAT5 signaling, PD-1 ablated memory CD8 T cells were significantly impaired in their ability to

homeostatically proliferate both in vitro in response to stimulation with IL-7 ($P<0.05$, Fig. 4C) and IL-15 ($P<0.01$, Fig. 4C), and in vivo when adoptively transferred into antigen-free naïve mice ($P<0.01$ in spleen and lung, $P<0.05$ in lymph node and liver, Fig. 4D, fig. S4B). Whereas purified WT memory CD8 T cells progressed normally through increasing rounds of homeostatic proliferation with increasing days, PD-1-deficient cells minimally diluted the CFSE dye (Fig. 4D, fig. S4B), and did not show division-associated increases in cellular DNA content (fig. S4C). These memory homeostasis defects were apparently independent of differences in key transcription factors regulating effector and memory CD8 T cell fates such as T-box transcription factors T-bet and eomesodermin and B cell lymphoma 6 (Bcl-6) (fig. S4D). Thymic developmental defects were also inapparent in PD-1-ablated H-2D^{b}:GP33-specific TCR transgenic CD8 T cells, as indicated by similar splenic numbers (fig. S4E), and similar expression of key phenotypic markers in naïve WT and PD-1 ablated cells (fig. S4F). In addition to total WT and PD-1-deficient donor cell homeostasis (Fig. 4D), when we analyzed homeostatic proliferation in phenotypically similar (CD127^{Hi} or CD62L^{Hi}) memory subsets known to homeostatically proliferate, we noted that PD-1-deficient cells were intrinsically impaired in their ability to undergo homeostatic proliferation regardless of their CD127^{Hi} or CD62L^{Hi} status (Fig. 4E) as late as about 70 days after infection (about 50 days after transfer into naïve mice). Defective homeostatic proliferation in the absence of PD-1 was associated with significant attrition of memory CD8 T cells in all lymphoid (spleen, $P<0.01$; lymph node, $P<0.05$) and nonlymphoid (lung, $P<0.01$; liver, $P<0.05$) compartments evaluated (Fig. 4F, fig. S4B). In addition to reduced numbers, PD-1-deficient T_{CM} cells also expressed less of the anti-apoptotic molecule, Bcl-2 (fig. S4G), though no differences were apparent for classic cell death markers including Fas, Caspase-3 or Bim (fig. S4H). Together, these studies demonstrate a critical role of PD-1 in regulating optimal antigen-independent homeostatic maintenance properties of quiescent memory CD8 T cells.

PD-1 signals regulate memory CD8 T cell metabolic programs during homeostasis.

Homeostatic maintenance of memory CD8 T cells is critically linked to their metabolic state. Transition of CD8 T cells from cytotoxic effector to quiescent memory state is associated with a metabolic switch to reduced glycolysis and increased fatty acid oxidation (73). Given that PD-1 is implicated in regulation of glycolytic metabolism during activation (41), we asked if the increased death of PD-1-deficient memory-fated cells during antigen-independent homeostasis was related to metabolic dysregulation, thus leading to impaired homeostatic proliferation and cell survival. To address this hypothesis, we purified PD-1 sufficient and deficient memory CD8 T cells at day 22 after infection (when WT memory CD8 T cells typically manifest homeostatic proliferation, and adequate numbers of PD-1-deficient cells may be still procured) and conducted a Seahorse extracellular flux assay (Fig. 5A to D) and metabolomics assessment (Fig. 5E). PD-1-deficient memory CD8 T cells exhibited more glycolytic and tricarboxylic acid (TCA) cycle flux (measured by extracellular acidification rate, ECAR) as well as oxidative phosphorylation (OXPHOS, measured by oxygen consumption rate, OCR) than their WT counterparts (Fig. 5A to D), and had a slightly increased spare respiratory capacity (SRC) in the presence of glucose as the energy substrate (Fig. 5A, fig. S5A). Analogous to PD-1-mediated suppression of glycolytic flux during TCR-induced activation (41), our observations of increased aerobic

glycolysis in PD-1-deficient memory CD8 T cells are intriguing since memory CD8 T cells typically persist in the absence of cognate antigen. Hence, we sought to extend these findings by determining whether PD-1-dependent glucose influx was impacted by homeostatic signals. Consistent with increased glucose oxidation, memory CD8 T cells lacking PD-1 were more efficient than WT cells at glucose uptake directly after isolation (Fig. 5B). Subsequent TCR stimulation or common γ-chain signaling led to induction of glucose uptake in both WT and PD-1 deficient memory cells (Fig. 5B), albeit PD-1 deficient memory cells retained higher glucose uptake properties than WT memory CD8 T cells (Fig. 5B). These data suggest a glycolysis regulatory role of PD-1 in memory development or homeostasis.

Although effector cells depend more on glucose-driven metabolism to meet their anabolic bioenergetic demands, naïve and memory CD8 T cells rely primarily on fatty acid oxidation (74). Hence, we next assessed the impact of PD-1 on fatty acid β-oxidation in memory CD8 T cells. We observed minimal glycolytic flux in WT and PD-1-deficient memory CD8 T cells in the presence of fatty acids as the sole energy substrate (Fig. 5C). However, loss of T cell-specific PD-1 signals resulted in impaired fatty acid oxidation by memory CD8 T cells, as evidenced by significantly lower OCR ($P<0.001$, Fig. 5C). Consistent with reduced fatty acid oxidation and possibly increased fatty acid synthesis due to enhanced glycolysis, PD-1 ablated memory CD8 T cells possessed higher fatty acid content when evaluated directly ex vivo (Fig. 5D), and also following stimulation with IL-2, IL-7, IL-15 or cognate antigen (Fig. 5D). These observations suggest that PD-1 promotes catabolic programs that drive utilization of fatty acid energy substrates in memory CD8 T cells. In agreement with the seahorse data, PD-1 ablated memory CD8 T cells showed significant upregulation of glycolytic intermediates pyruvate and lactate ($P<0.05$, Fig. 5E). PD-1 ablated memory CD8 T cells also exhibited decreased abundance of mitochondrial fatty acid oxidation cofactors acetylcarnitine and carnitine ($P<0.05$, Fig. 5E). Reduced fatty acid oxidation in PD-1 ablated memory CD8 T cells was also associated with higher concentrations of oxidized glutathione and lower concentrations of reduced glutathione (Fig. 5E), thus possibly rendering the cell more susceptible to oxidative damage.

To determine whether PD-1 signals are actively required during the memory maintenance phase to regulate their metabolism, we conducted antibody-mediated blockade of PD-1 signals in fully-differentiated WT memory CD8 T cells (Fig. 5F). Similar to PD-1-deficient memory CD8 T cells (Fig. 5A), abrogation of PD-1 signals under homeostatic conditions led to increased ECAR and OCR in the presence of glucose energy substrate (Fig. 5G and H). Metabolic perturbation of memory CD8 T cells upon PD-1 blockade was associated with limited decline in cell numbers (fig. S5B), the slow rate of homeostatic proliferation (intermitotic interval period of 50 days (75)). Consistent with increased contraction of PD-1-deficient cells (Fig. 3C), PD-1 blockade during contraction also led to decreased memory CD8 T cells (fig. S5C). In contrast, antibody blockade during the expansion phase did not result in a decline in memory numbers (fig. S5D). This is consistent with our in-depth effector differentiation analyses. Consistent with similar programming of effector CD8 T cells responses in the presence or absence of PD-1, WT and PD-1 ablated effector CD8 T cells exhibited similar mitochondrial mass and membrane potential at the peak of CTL expansion (fig. S5E). However, following antigen clearance, PD-1-deficient T cells exhibited

reduced mitochondrial potential as well as mitochondrial mass at day 22 (fig. S5E, $P<0.05$). These mitochondrial aberrancies were evident at day 22 after infection, when memory homeostasis manifests, both in total H-2D^{b}:GP33-specific CD8 T cells, as well as in the CD127^{Hi} KLRG-1^{Lo} memory-fated cells ($P<0.05$, fig. S5F). Collectively, these data support the notion that memory metabolic properties are likely not programmed by PD-1 signals during priming and expansion phase. Nonetheless, our metabolic assessments establish a critical role of PD-1 signals in suppressing the usage of glucose for energy generation, and in promoting fatty acid synthesis to support long-term homeostatic maintenance of memory CD8 T cells through fatty acid oxidation. More directed future studies involving conditional, stage-specific ablation of PD-1 will enable precise delineation of the relative contributions of PD-1 inhibitory signals during the distinct early CD8 T cell memory programming versus late homeostasis phases.

Attenuation of glycolysis through rapamycin reverses the memory survival defects associated with PD-1 deficiency.

Increased glycolysis and fatty acid content in PD-1-deficient memory CD8 T cells demonstrate a role for PD-1 in promoting the switch from glycolysis to fatty acid oxidation during memory maintenance. We next sought to investigate whether these metabolic differences might be functionally relevant in memory CD8 T cell survival, and whether the metabolic changes were mediated through mTOR. To address this question we administered rapamycin (Fig. 6A), a clinically approved drug that inhibits mTOR dependent glycolysis (76). The prediction was that suppression of aberrant glycolysis by blocking excessive mTOR signaling will rescue the memory defect in the absence of PD-1 in vivo.

To specifically focus on the memory differentiation phase, we started rapamycin treatment at about 6 days after acute LCMV infection, when virus is controlled. As shown previously (77), rapamycin treatment exerted beneficial effects on WT CD8 T cell memory survival in lymphoid organs (Fig. 6B to D, fig. S6A) through upregulation of Bcl-2 (Fig. 6E, fig. S6B). However, PD-1 deficient CD8 T cells responded more vigorously to rapamycin treatment and were found at significantly higher numbers, notably in the lymphoid organs (spleen, $P<0.001$; bone marrow, $P<0.01$, Fig. 6D, fig. S6A). Improved memory CD8 T cell numbers in the spleen and the bone marrow (but not lung and liver) during the short window of rapamycin treatment (days 6-33) is consistent with lymphoid organs being the primary niches of homeostatic memory maintenance as compared to non-lymphoid sites. In addition to overall memory numbers, rapamycin treatment increased the frequency of CD62L^{Hi} (Fig. 6F) and CD127^{Hi} (Fig. 6G) memory CD8 T cells regardless of PD-1 expression. However, the fold increase of CD127^{Hi} memory CD8 T cells was higher for PD-1-deficient T cells as compared to WT T cells following rapamycin treatment. Rapamycin treatment also reduced the frequency of terminally differentiated KLRG-1^{Hi} cells (Fig. 6H) in WT cells, as shown previously (77). In comparison to WT cells, PD-1-deficient memory CD8 T cells showed a significantly greater fold decrease of terminally differentiated KLRG-1^{Hi} cells following rapamycin treatment ($P<0.01$ Fig 6H). Nonetheless, memory CD8 T cell function, as assessed by polyfunctionality (or the ability to coproduce multiple cytokines) was largely the same in WT and PD-1 ablated CD8 T cells, and remained unaffected by rapamycin treatment (fig. S6C). We next determined if rescue of PD-1 ablated memory

CD8 T cell by rapamycin was associated with a concomitant reduction in glycolytic rate. Seahorse analysis revealed a significant reduction of ECAR upon rapamycin treatment in PD-1 ablated memory CD8 T cells, similar to WT cells ($P<0.05$, Fig. 6I). Collectively, metabolic dysregulation following PD-1 blockade during memory and rapamycin-mediated rescue of metabolic defects and memory numbers in PD-1-deficient cells, support a link between PD-1 inhibitory signals and CD8 T cell memory homeostasis through regulation of mTOR-dependent metabolic pathways (fig. S6D).

PD-1 checkpoint blockade immunotherapy during chronic infection causes attrition of pre-existing functional memory CD8 T cells.

PD-1 checkpoint blockade immunotherapy has offered much success in treating chronic viral infections and tumors by reinvigorating the exhausted virus- or tumor-reactive T cells (78). Our data show that functionally potent memory CD8 T cells generated in response to acute infections or immunizations express PD-1 at higher than naïve abundance, but still lower than the canonical exhausted cells, which are amenable to rescue by PD-1 blockade. We next sought to determine if PD-1 checkpoint blockade during chronic infection might exert side effects on pre-existing CD8 T cell memory established in response to a prior infection, and lead to bystander memory attrition. To investigate this, we generated ovalbumin (OVA) peptide-specific memory CD8 T cells in response to LM-OVA inoculation (Fig. 7A). These OVA-memory CD8 T cell-bearing mice were subsequently infected with chronic LCMV after about 60-75 days post-LM-OVA inoculation. OVA memory CD8 T cell-bearing mice were treated with anti-PD-1 or anti-PD-L1 antibody blockade, and bystander OVA-specific memory CD8 T cells were assessed for their numbers and functional properties (Fig. 7A). As expected, prior to PD-1 checkpoint blockade immunotherapy, OVA-specific memory CD8 T cells expressed intermediate PD-1 (Fig. 7B). On the other hand, owing to their history of chronic antigenic stimulation, CD8 T cells specific to the LCMV GP33 or GP276 epitopes were PD-1^{hi} (Fig. 7B). PD-1 or PD-L1 checkpoint blockade resulted in expansion of functionally reinvigorated LCMV-specific T cells, associated with reduced viral loads as previously described (7) (fig. S7A and B). However, contrary to the exhausted LCMV-specific cells, resting OVA-specific memory CD8 T cell numbers declined in both lymphoid and nonlymphoid sites after PD-1 or PD-L1 antibody treatment (Fig. 7C and D, fig. S7C), but largely retained their phenotypic and functional properties (Fig. 7C, fig. S7D and E), as shown by similar expression of CD127, KLRG-1, and similar production of IFN-γ, TNF-α and IL-2 upon antigenic restimulation (fig. S7D and E). Consistent with increased contraction of overall CD8 T cell memory population in the absence of T cell-specific PD-1 signals, generalized antibody-mediated PD-1 blockade did not result in any substantial alterations in the overall composition of memory subsets (Fig. 7C, fig. S7D). In summary, consistent with our findings of memory attrition upon CD8 T cell-specific PD-1 ablation, our observations that quiescent bystander memory CD8 T cells undergo attrition during PD-1 checkpoint blockade therapy during chronic infection support the possibility of a clinically relevant role of PD-1 signals in the long-term maintenance of functional CD8 T cell immune memory.

Discussion

The main goal of this study was to investigate the T cell-intrinsic role of PD-1 in memory CD8 T cell development. PD1 and PD-L1 antibody blockade causes systemic immune perturbations, and long-term treatment has been shown to induce autoimmunity in multiple clinical studies (79-81). Hence, we engaged the strategy of specifically ablating PD-1 on a fraction of antigen-specific CD8 T cells to compare memory differentiation of WT and PD-1-deficient CD8 T cells in the same infected host. By bypassing issues of systemic immune perturbations associated with global antibody-mediated blockade or germline deletions of PD-1 or PD-L1, this study also normalizes for any differences in immune milieu that might result from altered expansion, effector function and viral control. In this controlled setting, our studies of T cell specific loss of PD-1 signals show that: (i) during early stages of T cell priming, when PD-1 expression is most highly induced, it is largely dispensable for T cell activation, early proliferation and effector differentiation, (ii) during later stages of CTL expansion, PD-1 mediates modest attenuation of clonal expansion and effector differentiation, and (iii) PD-1 is critical for generating optimal numbers of memory CD8 T cells. By integrating phenotypic, functional, metabolomic and transcriptomic data, this study further offers new insight into how T cell-specific PD-1 signals promote long-term memory homeostasis through regulation of mTOR-dependent glucose oxidation, and enhancement of fatty acid oxidation. Moreover, this study expands into the translational realm by suggesting a risk for bystander CD8 T cell memory attrition during PD-1 checkpoint blockade immunotherapy.

Consistent with a largely inhibitory role of PD-1 in a variety of chronic and acute viral infections (12, 39, 44-46, 48), our studies show limited inhibition of T cell activation and effector CD8 T cell responses in the context of CD8 T cell-specific PD-1 deficiency. Our study further found a critical role of PD-1 in promoting the survival of memory-fated cells in distinct viral (LCMV and VACV) and bacterial (LM) infections. Enrichment of apoptosis gene signatures in PD-1-deficient effector CD8 T cells suggest that contraction properties are programmed by PD-1 during effector expansion. These findings have been recently extended to respiratory viral infections as well (48), and are consistent with a previous report of increased expansion followed by a faster decay rate for PD-1 knockout cells than WT cells in VACV infection (52). Nonetheless, more pronounced inhibition of effector responses in lung were reported by Pauken et al. (48) during respiratory viral infections, and the fold decline in antigen-specific CD8 T cell numbers in the absence of PD-1 is variable across infection models. These differences may be ascribed to disease model specific variations in effector differentiation-driving factors such as antigen persistence, inflammation, expression of PD-1 ligands, and subsets of antigen presenting cells and regulatory cells in distinct tissue sites that might uniquely intersect with PD-1 signals.

Memory defects in PD-1-deficient CD8 T cells were related to homeostatic proliferation and metabolic differences in the absence of antigen. Functional properties such as coproduction of multiple cytokines upon restimulation with cognate antigen and secondary recall expansion potential remained unaltered by the loss of PD-1 signals, indicating an independent regulation of these memory properties. It is possible that other inhibitory signals (such as Lymphocyte-Activation Gene 3 [LAG-3] or CD160) may compensate for

the loss of PD-1 to rescue memory CD8 T cells functional aspects to varying extents (82). In comparison to chronic LCMV infection, where CD8 T cell-specific PD-1 ablation was associated with an increase in the numbers of antigen-specific CD8 T cells and progressive loss of function (12), we observed a modest enhancement of CTL expansion yet loss of memory with preservation of polyfunctionality in acute infection. These differences in acute and chronic antigen settings might be ascribed to augmented expression of PD-1 ligands with persisting antigen and inflammation, thus rendering inhibitory signals more dominant at later stages of CTL expansion in chronic infection. In agreement with this, type-I interferons, which are potent inducers of PD-L1, have been found to exhibit elevated expression during chronic compared to acute LCMV infection, and blockade of IFN-I signaling leads to reduction of PD-L1 and control of persistent LCMV infection (83, 84).

Our data show that loss of PD-1 is associated with altered homeostatic maintenance, increased aerobic glucose metabolism and impaired fatty acid metabolism through mTOR. Inhibition of mTOR by rapamycin reversed the metabolic defects, and also partially rescued the CD8 T cell memory survival defects associated with loss of PD-1. Consistent with availability of homeostatic signals in the bone marrow (85-87), our studies show maximal rescue of memory numbers in the bone marrow. These findings implicate a potential involvement of the PD-1/mTOR axis in CD8 T cell memory, as in case of T cell activation (41), effector differentiation (39) and exhaustion as well (88, 89).

Considering the increasing promise of PD-1 blockade in reversing CD8 T cell exhaustion and providing beneficial therapeutic effects during chronic infections and in a variety of cancers in the clinic, these studies bear clinical implications. Our data showing decline in bystander memory CD8 T cell numbers following PD-1 checkpoint blockade during chronic LCMV infection suggest possible loss of protective immunity to prior infections and vaccinations following checkpoint blockade immunotherapy in the clinic. Additionally, loss of PD-1 inhibition might lead to augmentation of pathogenic immune responses as suggested by recrudescence of tuberculosis in two cancer patients following PD-1 checkpoint blockade immunotherapy (90). A lower magnitude of memory attrition by antibody blockade during homeostasis, and in the checkpoint blockade therapeutic setting, compared to PD-1 ablation model, might be ascribed to relatively short window of blockade in the face of long intermitotic division times during homeostatic proliferation (75). Additionally, inefficient antibody penetration into memory niches and infection-related compensatory factors might also mitigate the effect.

There are limitations to our study. Antibody-mediated blockade of PD-1 signals specifically during expansion, contraction, or memory maintenance phases implicate a role for PD-1 inhibition during contraction and memory maintenance phases. Likewise, rapid induction of metabolic differences following PD-1 blockade during memory support a requirement of PD-1 signals during memory phase. These findings are consistent with a recent study noting lack of evident memory defects in respiratory infections when PD-1 signals were blocked only during expansion (48). Nonetheless, future studies involving conditional stage-specific ablation of PD-1 in effector or memory CD8 T cells will provide conclusive insights into stage-specific regulation of memory homeostatic properties by PD-1 during expansion, contraction and memory maintenance phases. The impact of PD-1 blockade immunotherapy

on bystander memory CD8 and CD4 T cells might vary depending on the immunologic milieu. Hence, future studies into bystander memory CD8 T cell attrition under distinct infection and cancer models with unique inflammatory microenvironments will test the breadth of clinical implications of PD-1 blockade, and further illuminate the mechanistic bases of memory attrition. Our data demonstrate the involvement of the PD-1/mTOR axis in metabolic regulation of memory CD8 T cells. However, the precise molecular mediators downstream od PD-1 and mTOR need to be fully elucidated. Moreover, the T cell-extrinsic signals (antigen, inflammatory or homeostatic cytokines) that are suppressed by PD-1 to support the metabolic transition of CD8 T cells from effector to memory programs also require further categorical studies. Likewise, CD28 costimulation plays an important role in rejuvenation of exhausted CD8 T cells by PD-1 checkpoint blockade immunotherapy (27, 28). Whether CD28 exerts a role in PD-1 mediated metabolic regulation of CD8 T cell memory remains to be investigated in future studies.

In conclusion, these studies present a model of PD-1-dependent CD8 T cell memory longevity through metabolic regulation. Metabolic regulation of quiescent yet functional memory CD8 T cells through PD-1 and PD-L1 signaling represents a regulatory pathway that may be exploited to manipulate the durability of CD8 T cell immune memory. These studies are relevant to CD8 T cell memory outcomes following immunizations and acute infections, and possibly during checkpoint blockade therapy.

Materials and Methods

Study design

The overall objective of the study was to query the CD8 T cell specific role of PD-1 in memory responses. To address this adoptive co-transfer strategy of $H2D^b$:GP33 antigen-specific WT and PD-$1^{-/-}$ CD8 T cells in the same C57Bl/6 host was engaged. Studies were conducted using distinct precursor frequencies (10^2 to 10^5) of $H2D^b$:GP33 antigen-specific CD8 T cells. To query stage-specific effects of PD-1 signaling , antibody blockade of PD-1 or PD-L1 was conducted in infected mice. Absolute numbers, phenotypic, functional, metabolic and gene expression assessments were conducted at distinct stages of CD8 T cell differentiation – expansion and effector differentiation, contraction and memory homeostasis. Based on power analysis, sample size of 3 to 5 mice were used for independent repeats for desired power of 0.80 and type I error rate of 0.05 to detect at least 20% difference in means. Experimental end-points were determined at pre-defined naïve, effector or memory stages of CD8 T cell differentiation. In antibody blockade experiments, mice were randomly assigned to untreated or treated groups. Experimentation and assessment of outcomes were not blinded.

Mice

C57BL/6 mice (Thy1.2^+, Thy1.1^+, or Ly5.1^+) were purchased from the Jackson Laboratory. Thy1.1^+ P14 mice bearing the H-$2D^b$:GP33 epitope-specific TCR were fully backcrossed to C57BL/6 mice and were maintained in our animal colony. PD-$1^{-/-}$ P14 mice were generated via breeding of PD-$1^{-/-}$ mice with WT P14 mice until the PD-$1^{-/-}$ locus was homozygous on a P14 background. All animals were used in accordance with the Seattle

Children's Research Institute Animal Care and Use Committee guidelines. For generating chimeric mice, WT and PD-$1^{-/-}$ P14 cells were co-transferred intravenously in equal numbers. For CFSE experiments, $0.5x10^6$-$1.0x10^6$ antigen-specific WT and PD-$1^{-/-}$ P14 cells were transferred. For analysis of effector and memory CD8 T cell responses over time, WT and PD-$1^{-/-}$ P14 cells were co-transferred at $2x10^3$ (low dose) or $5x10^4$ (high dose) antigen-specific cells.

Virus and Bacterial Propagation and Infection

Armstrong and Cl-13 strains of LCMV and recombinant Listeria monocytogenes (LM-GP33, LM-OVA) were propagated and titered in baby hamster kidney (BHK) cell line and brain heart infusion media, respectively, as described previously (91, 92). Pathogens were used for infections as follows: mice were injected intraperitoneally with 2×10^5 plaque-forming units (PFU) $LCMV_{Arm}$ to establish an acute infection; to establish chronicity, mice were infected intravenously with 2×10^6 PFU LCMV; Vaccina-GP33 virus (gift from Dr. Rafi Ahmed, Emory University) was injected intravenously with 2×10^6 PFU; for primary LM infections, mice were infected with 10,000 colony-forming units (CFU) LM-OVA or 20,000 CFU LM-GP33 intravenously; for secondary expansion studies, mice were infected intravenously with 30,000 CFU LM-GP33.

Flow cytometry

All antibodies were purchased from BioLegend with the exception of granzyme B (Invitrogen). MHC class I tetramers were made as described previously (93), and cells were stained for surface or intracellular proteins and cytokines. For analysis of intracellular cytokines, $2x10^6$ red blood cell (RBC)-lysed crude splenocyte preparations were stimulated with 0.2μg/ml GP33-41 peptide (GenScript) in the presence of brefeldin A (Sigma-Aldrich) for 5 hours, followed by surface staining for CD8 (Clone 53.67, brilliant violet (BV)650 1:100), Ly5.1 (Clone A20, fluorescein isothiocyanate (FITC) 1:100, BV421 1:100), Thy1.1 (Clone OX-7, peridinin chlorophyll protein (PerCP) 1:300), or Thy1.2 (Clone 30-H12, pacific blue 1:200, alexa fluor 700 1:200), PD-1 (Clone RMP1-30, Phycoerythrin (PE)-Cy7 1:100), CD127 (Clone A7R34, PE 1:100, BV421 1:100), KLRG-1 (Clone 2F1, allophycocyanin (APC) 1:100, FITC 1:100), CD62L (Clone MEL-14, pacific blue 1:75, A700 1:75) and intracellular staining for IFN-γ (Clone XMG1.2, FITC 1:100), TNF-α, (Clone MP6-XT22, APC 1:100) or IL-2 (Clone JES6-584, PE 1:100). All antibody staining was conducted on ice for 45 minutes. Analysis of pS6 was conducted by phosphoflow staining of samples either directly after isolation or following in vitro stimulation for 30 minutes with GP33 peptide as described previously (94). Flow cytometric analysis was performed on an LSRII Fortessa (BD Biosciences). Single cell suspensions of spleen cells, lymph nodes, lungs, livers or peripheral blood mononuclear cells (PBMCs) from mice were prepared and staining was carried out as described previously (94). To differentiate between circulatory and resident CD8 T cells in harvested organs, mice were injected with 3 μg (in 500μl) fluorochrome-conjugated anti-CD8β (Clone YTS156.7.7, BioLegend) intravenously and euthanized 4 minutes after antibody delivery. Organs were subsequently harvested and processed in a dark environment. Cells were stained and incubated with marker antibodies as described above in a dark environment. The cells were acquired via flow cytometry within

24 hours and those positive for CD8β were considered to be the circulatory population. The resident population was not marked with the CD8β antibody.

Proliferation analyses

For analysis of cell proliferation, splenocytes were first labeled with CFSE (Invitrogen) at a concentration of 10×10^6 cells/mL and 5μM CFSE in RPMI-1640 medium. For in vitro proliferation analyses, CFSE-labeled LCMV memory CD8 T cells were cultured at 37°C with IL-7, IL-15, or GP33-41 peptide in RPMI-1640 supplemented with 10% fetal bovine serum. For in vivo proliferation analyses, 1×10^6 CFSE labeled memory CD8 T cells were adoptively transferred into naïve C57BL/6 recipients and bled weekly in an antigen free environment.

Metabolic assays

For Seahorse analysis, antigen-specific CD8 T cells were purified from splenocytes using EasySep (Stemcell Technologies) or MojoSort (BioLegend) positive biotin selection kits. Cells were plated at $4x10^5$ (XF 24) or $1.5x10^5$ (XF 96) per well using poly-L-lysine adhesive (Sigma). Agilent XF 24 and 96 analyzers were utilized. Oligomycin, Trifluoromethoxy carbonylcyanide phenylhydrazone (FCCP), Rotenone/Antimycin A (Agilent Seahorse XF Cell Mito Stress Test Kit), 2-deoxyglucose (VWR), and etomoxir (Sigma-Aldrich) were used to probe different metabolic assays. Mitochondrial assays were performed with samples after isolation using tetramethylrhodamine ethyl ester (TMRE) and Mitotracker (Invitrogen) per manufacturer's instructions. Fluorescent glucose analog N-(7-Nitrobenz-2-oxa-1,3-diazol-4-yl)Amino)-2-Deoxyglucose (2-NBDG) (Invitrogen) was used for glucose flux analyses, and 4,4-Difluoro-1,3,5,7,8-Pentamethyl-4-Bora-3a,4a-Diaza-s-Indacene (BODIPY 493/503) (Invitrogen) was used for fatty acid content analyses per manufacturer's instructions. For metabolomics analysis, cells were FACS purified and stored in 80% methanol to quench metabolism. Cytosolic metabolites were isolated and dried using Speedvac. Samples were sent to the Northwest Metabolomics Research Center for LC/TQ MS. Data were analyzed at Elucidata.

Antibody blockade

Mice were treated at indicated time points post-infection (as indicated in the figure legends). Mice were treated with 200 μg/mouse of anti-PD-1 (29F.1A12) or anti-PD-L1 (10F.9G2) (BioXcell) given intraperitoneally every third day in a total volume of 500μl. Similar volume of PBS was injected in control animals.

Rapamycin treatment

Mice received rapamycin daily by intraperitoneal injection starting at day 6 of $LCMV_{Arm}$ infection. Mice were treated with 600 μg/kg Rapamycin (Alfa Aesar) in sterile phosphate-buffered saline (PBS). Control mice were treated daily with sterile PBS.

Microarray Samples

WT ($5x10^4$ cells, Thy1.1/1.2) and PD-$1^{-/-}$ ($5x10^4$ cells, Thy1.1/1.1) CD8 T cells were adoptively cotransferred into naïve C57BL6 mice (Thy1.2/1.2), which were subsequently

infected with $2x10^5$ PFU $LCMV_{Arm}$. Splenocytes were isolated on day 7 post-infection and sorted for WT and PD-$1^{-/-}$ effector CD8 T cells. Sorted cells were resuspend in Trizol (Invitrogen). Subsequent cDNA, cRNA synthesis, and hybridization to mouse 430.2 microarray chips (Affymetrix) were performed according to the manufacturer's protocol as done previously (33). Raw data were normalized using the RMA package built within Genespring 7.0 (Agilent Technologies), and fold-change comparisons between the groups indicated in the figures were subsequently made. Microarray datasets (GSE181068) generated in this study have been made publicly available through the National Center for Biotechnology Information Gene Expression Omnibus (GEO) database. To test for the enrichment of effector and memory precursor signatures, GSEA was performed as previously described (35).

Statistical analysis

Paired or unpaired Student's t-test was used as indicated to evaluate differences between sample means. Paired analysis was conducted at indicated times after infection in experimental settings where WT and PD-$1^{-/-}$ CD8 T cells were cotransferred into the same host. Unpaired t-test was used to compare treated and untreated groups from in vitro or in vivo studies, or WT and PD-$1^{-/-}$ CD8 T cells in separate hosts at indicated times after infection. A one-way analysis of variance (ANOVA) with Tukey's post-hoc test was used for experiments with 3 or more groups to compare means across distinct groups. All statistical analyses were performed using GraphPad Prism 5 with default Gaussian distribution assumption for biological data from genetically inbred mice. P values of statistical significance are depicted by asterisks: * $P \leq 0.05$, ** $P \leq 0.01$, and *** $P \leq 0.001$ in the figures. In cases where statistically significant differences were not observed, no asterisk marks are included.

Supplementary Material

Refer to Web version on PubMed Central for supplementary material.

Acknowledgements:

The authors would like to thank Tasuku Honjo for the *pdcd1*$^{-/-}$ mice and Phil Morgan, Margaret Sedensky, and Kayser Ernst-Bernhard for discussions on the studies involving metabolic assays. We would also like to thank Shruti Bhise, Rucha Deo, and Laura Penny for technical assistance.

Funding:

This work was supported by research funding from the Seattle Children's Research Institute to SS and VK, Kelsey Dickson Team Science Courage Research Award Prostate Cancer Foundation to PN, and from the National Institutes of Health (AI132819 to SS and AI103748 to SS; AI154363 to VK; CA225517 to PN).

Data Availability:

All data associated with this study are in the paper or supplementary materials. Microarray datasets are available at the National Center for Biotechnology Information GEO database under accession number GSE181068.

References and Notes

1. Wherry EJ, T cell exhaustion. Nat Immunol 12, 492–499 (2011). [PubMed: 21739672]
2. Wherry EJ, Kurachi M, Molecular and cellular insights into T cell exhaustion. Nat Rev Immunol 15, 486–499 (2015). [PubMed: 26205583]
3. Blackburn SD et al. , Coregulation of CD8+ T cell exhaustion by multiple inhibitory receptors during chronic viral infection. Nat Immunol 10, 29–37 (2009). [PubMed: 19043418]
4. Sakuishi K et al. , Targeting Tim-3 and PD-1 pathways to reverse T cell exhaustion and restore anti-tumor immunity. J Exp Med 207, 2187–2194 (2010). [PubMed: 20819927]
5. Schildberg FA, Klein SR, Freeman GJ, Sharpe AH, Coinhibitory Pathways in the B7-CD28 Ligand-Receptor Family. Immunity 44, 955–972 (2016). [PubMed: 27192563]
6. Freeman GJ et al. , Engagement of the PD-1 immunoinhibitory receptor by a novel B7 family member leads to negative regulation of lymphocyte activation. J Exp Med 192, 1027–1034 (2000). [PubMed: 11015443]
7. Barber DL et al. , Restoring function in exhausted CD8 T cells during chronic viral infection. Nature 439, 682–687 (2006). [PubMed: 16382236]
8. Day CL et al. , PD-1 expression on HIV-specific T cells is associated with T-cell exhaustion and disease progression. Nature 443, 350–354 (2006). [PubMed: 16921384]
9. Petrovas C et al. , PD-1 is a regulator of virus-specific CD8+ T cell survival in HIV infection. J Exp Med 203, 2281–2292 (2006). [PubMed: 16954372]
10. Urbani S et al. , PD-1 expression in acute hepatitis C virus (HCV) infection is associated with HCV-specific CD8 exhaustion. J Virol 80, 11398–11403 (2006). [PubMed: 16956940]
11. Velu V et al. , Enhancing SIV-specific immunity in vivo by PD-1 blockade. Nature 458, 206–210 (2009). [PubMed: 19078956]
12. Odorizzi PM, Pauken KE, Paley MA, Sharpe A, Wherry EJ, Genetic absence of PD-1 promotes accumulation of terminally differentiated exhausted CD8+ T cells. J Exp Med 212, 1125–1137 (2015). [PubMed: 26034050]
13. Speiser DE, Ho PC, Verdeil G, Regulatory circuits of T cell function in cancer. Nat Rev Immunol 16, 599–611 (2016). [PubMed: 27526640]
14. Topalian SL, Drake CG, Pardoll DM, Targeting the PD-1/B7-H1(PD-L1) pathway to activate anti-tumor immunity. Curr Opin Immunol 24, 207–212 (2012). [PubMed: 22236695]
15. Topalian SL et al. , Safety, activity, and immune correlates of anti-PD-1 antibody in cancer. N Engl J Med 366, 2443–2454 (2012). [PubMed: 22658127]
16. Brahmer JR et al. , Safety and activity of anti-PD-L1 antibody in patients with advanced cancer. N Engl J Med 366, 2455–2465 (2012). [PubMed: 22658128]
17. Hamid O et al. , Safety and tumor responses with lambrolizumab (anti-PD-1) in melanoma. N Engl J Med 369, 134–144 (2013). [PubMed: 23724846]
18. Tumeh PC et al. , PD-1 blockade induces responses by inhibiting adaptive immune resistance. Nature 515, 568–571 (2014). [PubMed: 25428505]
19. Powles T et al. , MPDL3280A (anti-PD-L1) treatment leads to clinical activity in metastatic bladder cancer. Nature 515, 558–562 (2014). [PubMed: 25428503]
20. Herbst RS et al. , Predictive correlates of response to the anti-PD-L1 antibody MPDL3280A in cancer patients. Nature 515, 563–567 (2014). [PubMed: 25428504]
21. Yadav M et al. , Predicting immunogenic tumour mutations by combining mass spectrometry and exome sequencing. Nature 515, 572–576 (2014). [PubMed: 25428506]
22. Im SJ et al. , Defining CD8+ T cells that provide the proliferative burst after PD-1 therapy. Nature 537, 417–421 (2016). [PubMed: 27501248]
23. He R et al. , Follicular CXCR5- expressing CD8(+) T cells curtail chronic viral infection. Nature 537, 412–428 (2016). [PubMed: 27501245]
24. Shin H et al. , A role for the transcriptional repressor Blimp-1 in CD8(+) T cell exhaustion during chronic viral infection. Immunity 31, 309–320 (2009). [PubMed: 19664943]

25. Kao C et al. , Transcription factor T-bet represses expression of the inhibitory receptor PD-1 and sustains virus-specific CD8+ T cell responses during chronic infection. Nat Immunol 12, 663–671 (2011). [PubMed: 21623380]
26. Kurachi M et al. , The transcription factor BATF operates as an essential differentiation checkpoint in early effector CD8+ T cells. Nat Immunol 15, 373–383 (2014). [PubMed: 24584090]
27. Kamphorst AO et al. , Proliferation of PD-1+ CD8 T cells in peripheral blood after PD-1-targeted therapy in lung cancer patients. Proc Natl Acad Sci U S A 114, 4993–4998 (2017). [PubMed: 28446615]
28. Hui E et al. , T cell costimulatory receptor CD28 is a primary target for PD-1-mediated inhibition. Science 355, 1428–1433 (2017). [PubMed: 28280247]
29. Paley MA et al. , Progenitor and terminal subsets of CD8+ T cells cooperate to contain chronic viral infection. Science 338, 1220–1225 (2012). [PubMed: 23197535]
30. Utzschneider DT et al. , T Cell Factor 1-Expressing Memory-like CD8(+) T Cells Sustain the Immune Response to Chronic Viral Infections. Immunity 45, 415–427 (2016). [PubMed: 27533016]
31. Ribas A, Wolchok JD, Cancer immunotherapy using checkpoint blockade. Science 359, 1350–1355 (2018). [PubMed: 29567705]
32. Kalia VA, R.; Sarkar S, CD8 T cell memory to pathogens. Encyclopedia of Immunobiology; Editors: Dr. Michale Ratcliffe Elsevier (1st Edition., 2016), (2016).
33. Kalia V, Penny LA, Yuzefpolskiy Y, Baumann FM, Sarkar S, Quiescence of Memory CD8(+) T Cells Is Mediated by Regulatory T Cells through Inhibitory Receptor CTLA-4. Immunity 42, 1116–1129 (2015). [PubMed: 26084026]
34. Kalia V et al. , Prolonged interleukin-2Ralpha expression on virus-specific CD8+ T cells favors terminal-effector differentiation in vivo. Immunity 32, 91–103 (2010). [PubMed: 20096608]
35. Sarkar S et al. , Functional and genomic profiling of effector CD8 T cell subsets with distinct memory fates. J Exp Med 205, 625–640 (2008). [PubMed: 18316415]
36. Laidlaw BJ et al. , Production of IL-10 by CD4(+) regulatory T cells during the resolution of infection promotes the maturation of memory CD8(+) T cells. Nat Immunol 16, 871–879 (2015). [PubMed: 26147684]
37. Joshi NS et al. , Inflammation directs memory precursor and short-lived effector CD8(+) T cell fates via the graded expression of T-bet transcription factor. Immunity 27, 281–295 (2007). [PubMed: 17723218]
38. Chang JT et al. , Asymmetric T lymphocyte division in the initiation of adaptive immune responses. Science 315, 1687–1691 (2007). [PubMed: 17332376]
39. Ahn E et al. , Role of PD-1 during effector CD8 T cell differentiation. Proc Natl Acad Sci U S A 115, 4749–4754 (2018). [PubMed: 29654146]
40. Chemnitz JM, Parry RV, Nichols KE, June CH, Riley JL, SHP-1 and SHP-2 associate with immunoreceptor tyrosine-based switch motif of programmed death 1 upon primary human T cell stimulation, but only receptor ligation prevents T cell activation. J Immunol 173, 945–954 (2004). [PubMed: 15240681]
41. Patsoukis N et al. , PD-1 alters T-cell metabolic reprogramming by inhibiting glycolysis and promoting lipolysis and fatty acid oxidation. Nat Commun 6, 6692 (2015). [PubMed: 25809635]
42. Brown KE, Freeman GJ, Wherry EJ, Sharpe AH, Role of PD-1 in regulating acute infections. Curr Opin Immunol 22, 397–401 (2010). [PubMed: 20427170]
43. Odorizzi PM, Wherry EJ, Inhibitory receptors on lymphocytes: insights from infections. J Immunol 188, 2957–2965 (2012). [PubMed: 22442493]
44. Telcian AG et al. , RSV-induced bronchial epithelial cell PD-L1 expression inhibits CD8+ T cell nonspecific antiviral activity. J Infect Dis 203, 85–94 (2011). [PubMed: 21148500]
45. Iwai Y, Terawaki S, Ikegawa M, Okazaki T, Honjo T, PD-1 inhibits antiviral immunity at the effector phase in the liver. J Exp Med 198, 39–50 (2003). [PubMed: 12847136]
46. Lafon M et al. , Detrimental contribution of the immuno-inhibitor B7-H1 to rabies virus encephalitis. J Immunol 180, 7506–7515 (2008). [PubMed: 18490751]

47. Frebel H et al. , Programmed death 1 protects from fatal circulatory failure during systemic virus infection of mice. J Exp Med 209, 2485–2499 (2012). [PubMed: 23230000]
48. Pauken KE et al. , The PD-1 Pathway Regulates Development and Function of Memory CD8(+) T Cells following Respiratory Viral Infection. Cell Rep 31, 107827 (2020). [PubMed: 32610128]
49. Rowe JH, Johanns TM, Ertelt JM, Way SS, PDL-1 blockade impedes T cell expansion and protective immunity primed by attenuated Listeria monocytogenes. J Immunol 180, 7553–7557 (2008). [PubMed: 18490756]
50. Talay O, Shen CH, Chen L, Chen J, B7-H1 (PD-L1) on T cells is required for T-cell-mediated conditioning of dendritic cell maturation. Proc Natl Acad Sci U S A 106, 2741–2746 (2009). [PubMed: 19202065]
51. Xu D et al. , A potential new pathway for PD-L1 costimulation of the CD8-T cell response to Listeria monocytogenes infection. PLoS One 8, e56539 (2013). [PubMed: 23409193]
52. Allie SR, Zhang W, Fuse S, Usherwood EJ, Programmed death 1 regulates development of central memory CD8 T cells after acute viral infection. J Immunol 186, 6280–6286 (2011). [PubMed: 21525385]
53. Sarkar S et al. , Strength of stimulus and clonal competition impact the rate of memory CD8 T cell differentiation. J Immunol 179, 6704–6714 (2007). [PubMed: 17982060]
54. Marzo AL et al. , Initial T cell frequency dictates memory CD8+ T cell lineage commitment. Nat Immunol 6, 793–799 (2005). [PubMed: 16025119]
55. Badovinac VP, Haring JS, Harty JT, Initial T cell receptor transgenic cell precursor frequency dictates critical aspects of the CD8(+) T cell response to infection. Immunity 26, 827–841 (2007). [PubMed: 17555991]
56. Agata Y et al. , Expression of the PD-1 antigen on the surface of stimulated mouse T and B lymphocytes. Int Immunol 8, 765–772 (1996). [PubMed: 8671665]
57. Matloubian M, Kolhekar SR, Somasundaram T, Ahmed R, Molecular determinants of macrophage tropism and viral persistence: importance of single amino acid changes in the polymerase and glycoprotein of lymphocytic choriomeningitis virus. J Virol 67, 7340–7349 (1993). [PubMed: 7693969]
58. Wherry EJ et al. , Molecular signature of CD8+ T cell exhaustion during chronic viral infection. Immunity 27, 670–684 (2007). [PubMed: 17950003]
59. Duraiswamy J et al. , Phenotype, function, and gene expression profiles of programmed death-1(hi) CD8 T cells in healthy human adults. J Immunol 186, 4200–4212 (2011). [PubMed: 21383243]
60. Dolfi DV et al. , Increased T-bet is associated with senescence of influenza virus-specific CD8 T cells in aged humans. J Leukoc Biol 93, 825–836 (2013). [PubMed: 23440501]
61. Kaech SM et al. , Selective expression of the interleukin 7 receptor identifies effector CD8 T cells that give rise to long-lived memory cells. Nat Immunol 4, 1191–1198 (2003). [PubMed: 14625547]
62. Huster KM et al. , Selective expression of IL-7 receptor on memory T cells identifies early CD40L-dependent generation of distinct CD8+ memory T cell subsets. Proc Natl Acad Sci U S A 101, 5610–5615 (2004). [PubMed: 15044705]
63. Geltink RIK, Kyle RL, Pearce EL, Unraveling the Complex Interplay Between T Cell Metabolism and Function. Annu Rev Immunol 36, 461–488 (2018). [PubMed: 29677474]
64. Kalia V, Sarkar S, Regulation of Effector and Memory CD8 T Cell Differentiation by IL-2-A Balancing Act. Front Immunol 9, 2987 (2018). [PubMed: 30619342]
65. Pipkin ME et al. , Interleukin-2 and inflammation induce distinct transcriptional programs that promote the differentiation of effector cytolytic T cells. Immunity 32, 79–90 (2010). [PubMed: 20096607]
66. Refaeli Y, Van Parijs L, Alexander SI, Abbas AK, Interferon gamma is required for activation-induced death of T lymphocytes. J Exp Med 196, 999–1005 (2002). [PubMed: 12370261]
67. Badovinac VP, Messingham KA, Jabbari A, Haring JS, Harty JT, Accelerated CD8+ T-cell memory and prime-boost response after dendritic-cell vaccination. Nat Med 11, 748–756 (2005). [PubMed: 15951824]
68. Mehta AK, Gracias DT, Croft M, TNF activity and T cells. Cytokine 101, 14–18 (2018). [PubMed: 27531077]

69. Shin H, Blackburn SD, Blattman JN, Wherry EJ, Viral antigen and extensive division maintain virus-specific CD8 T cells during chronic infection. J Exp Med 204, 941–949 (2007). [PubMed: 17420267]
70. Utzschneider DT et al. , High antigen levels induce an exhausted phenotype in a chronic infection without impairing T cell expansion and survival. J Exp Med 213, 1819–1834 (2016). [PubMed: 27455951]
71. Kalia V, Sarkar S, Ahmed R, CD8 T-cell memory differentiation during acute and chronic viral infections. Adv Exp Med Biol 684, 79–95 (2010). [PubMed: 20795542]
72. Surh CD, Sprent J, Homeostasis of naive and memory T cells. Immunity 29, 848–862 (2008). [PubMed: 19100699]
73. Buck MD, Sowell RT, Kaech SM, Pearce EL, Metabolic Instruction of Immunity. Cell 169, 570–586 (2017). [PubMed: 28475890]
74. Buck MD, O'Sullivan D, Pearce EL, T cell metabolism drives immunity. J Exp Med 212, 1345–1360 (2015). [PubMed: 26261266]
75. Choo DK, Murali-Krishna K, Anita R, Ahmed R, Homeostatic turnover of virus-specific memory CD8 T cells occurs stochastically and is independent of CD4 T cell help. J Immunol 185, 3436–3444 (2010). [PubMed: 20733203]
76. Salmond RJ, mTOR Regulation of Glycolytic Metabolism in T Cells. Front Cell Dev Biol 6, 122 (2018). [PubMed: 30320109]
77. Araki K et al. , mTOR regulates memory CD8 T-cell differentiation. Nature 460, 108–112 (2009). [PubMed: 19543266]
78. McLane LM, Abdel-Hakeem MS, Wherry EJ, CD8 T Cell Exhaustion During Chronic Viral Infection and Cancer. Annu Rev Immunol 37, 457–495 (2019). [PubMed: 30676822]
79. Johnson DB et al. , Fulminant Myocarditis with Combination Immune Checkpoint Blockade. N Engl J Med 375, 1749–1755 (2016). [PubMed: 27806233]
80. Das R et al. , Early B cell changes predict autoimmunity following combination immune checkpoint blockade. J Clin Invest 128, 715–720 (2018). [PubMed: 29309048]
81. Pauken KE, Dougan M, Rose NR, Lichtman AH, Sharpe AH, Adverse Events Following Cancer Immunotherapy: Obstacles and Opportunities. Trends Immunol 40, 511–523 (2019). [PubMed: 31053497]
82. Johnnidis JB et al. , Inhibitory signaling sustains a distinct early memory CD8(+) T cell precursor that is resistant to DNA damage. Sci Immunol 6, (2021).
83. Wilson EB et al. , Blockade of chronic type I interferon signaling to control persistent LCMV infection. Science 340, 202–207 (2013). [PubMed: 23580528]
84. Teijaro JR et al. , Persistent LCMV infection is controlled by blockade of type I interferon signaling. Science 340, 207–211 (2013). [PubMed: 23580529]
85. Becker TC, Coley SM, Wherry EJ, Ahmed R, Bone marrow is a preferred site for homeostatic proliferation of memory CD8 T cells. J Immunol 174, 1269–1273 (2005). [PubMed: 15661882]
86. Di Rosa F, Pabst R, The bone marrow: a nest for migratory memory T cells. Trends Immunol 26, 360–366 (2005). [PubMed: 15978522]
87. Parretta E et al. , Kinetics of in vivo proliferation and death of memory and naive CD8 T cells: parameter estimation based on 5-bromo-2'-deoxyuridine incorporation in spleen, lymph nodes, and bone marrow. J Immunol 180, 7230–7239 (2008). [PubMed: 18490722]
88. Bengsch B et al. , Bioenergetic Insufficiencies Due to Metabolic Alterations Regulated by the Inhibitory Receptor PD-1 Are an Early Driver of CD8(+) T Cell Exhaustion. Immunity 45, 358–373 (2016). [PubMed: 27496729]
89. Scharping NE, Menk AV, Whetstone RD, Zeng X, Delgoffe GM, Efficacy of PD-1 Blockade Is Potentiated by Metformin-Induced Reduction of Tumor Hypoxia. Cancer Immunol Res 5, 9–16 (2017). [PubMed: 27941003]
90. Barber DL et al. , Tuberculosis following PD-1 blockade for cancer immunotherapy. Sci Transl Med 11, (2019).
91. Welsh RM, Seedhom MO, Lymphocytic choriomeningitis virus (LCMV): propagation, quantitation, and storage. Curr Protoc Microbiol Chapter 15, Unit 15A 11 (2008).

92. Jones GS, D'Orazio SEF, Listeria monocytogenes: cultivation and laboratory maintenance. Curr Protoc Microbiol 31, 9B 2 1–9B 2 7 (2013).

93. Murali-Krishna K et al. , Counting antigen-specific CD8 T cells: a reevaluation of bystander activation during viral infection. Immunity 8, 177–187 (1998). [PubMed: 9491999]

94. Khan AA, Penny LA, Yuzefpolskiy Y, Sarkar S, Kalia V, MicroRNA-17~92 regulates effector and memory CD8 T-cell fates by modulating proliferation in response to infections. Blood 121, 4473–4483 (2013). [PubMed: 23596046]

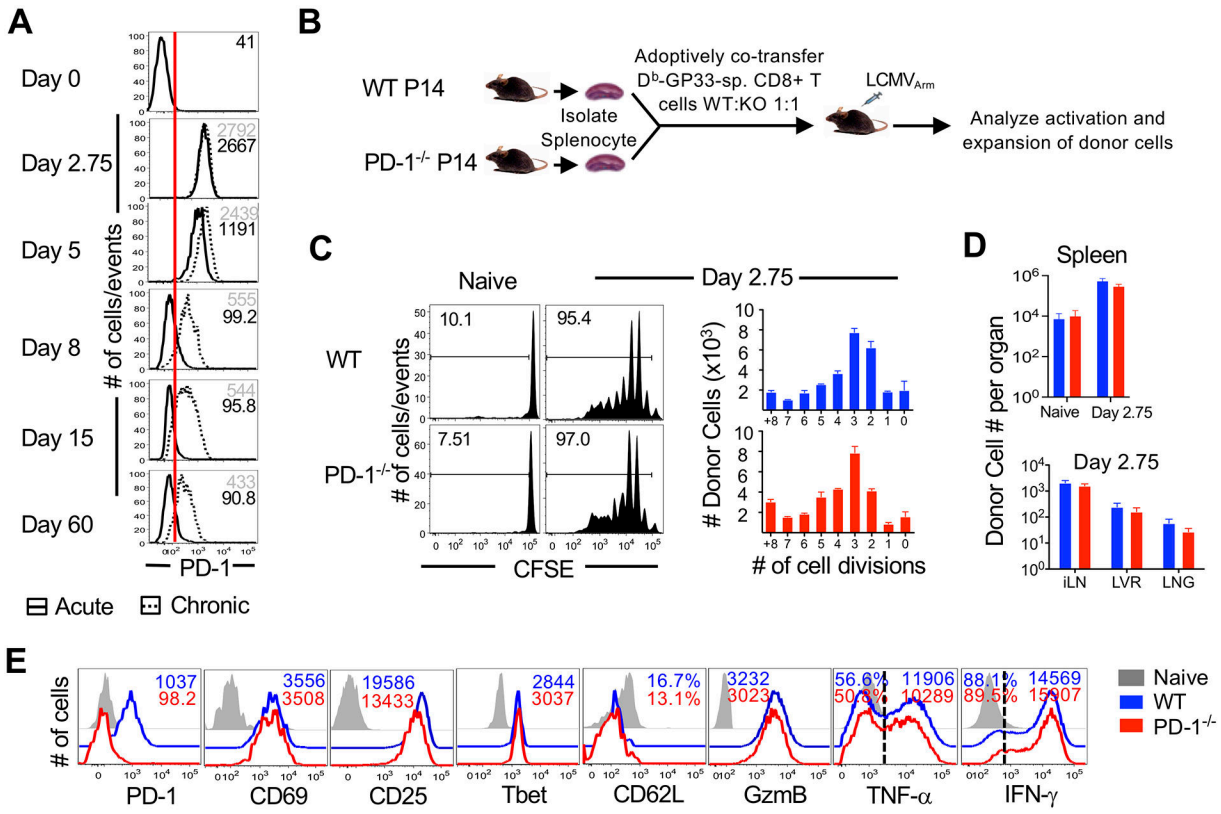

Figure 1. CD8 T cell-specific PD-1 deficiency does not impact the activation or proliferation of CD8 T cells during priming.

(A) WT P14 CD8 T cells were adoptively transferred into naive C57BL/6 mice ($2x10^3$ cells), which were subsequently infected with $LCMV_{Arm}$ as a model of acute infection or $LCMV_{CL-13}$ as a model of chronic infection. Histograms show PD-1 expression on donor antigen-specific CD8 T cells isolated from spleens at indicated days following acute (solid histogram; black numbers indicate mean fluorescence intensity (MFI) or chronic (dotted histogram; gray numbers indicate MFI) infection. Red line indicates the highest amount of PD-1 expression on naïve $H2D^b$:GP33-specific CD8 T cells. **(B)** Equal numbers of WT and PD-$1^{-/-}$ P14 CD8 T cells were adoptively co-transferred at 10^6 cells/mouse into C57BL/6 mice. Mice were infected with $LCMV_{Arm}$ and analyzed at day 2.75 post-infection. **(C)** Donor cells were CFSE labeled prior to adoptive transfer. Histograms are gated on donors and depict CFSE dilution at day 2.75 post-infection. Bar graphs show total numbers of WT and PD-$1^{-/-}$ donor antigen-specific CD8 T cells in spleen per cell division. **(D)** Bar graphs show total numbers of donor cells in naïve spleens (N) and spleen, inguinal lymph nodes (iLN), liver (LVR) and lung (LNG) tissues at day 2.75 post-infection. **E.** Histograms are gated on WT (blue) or PD-$1^{-/-}$ (red) antigen-specific CD8 T cells isolated from spleen; grey histograms show endogenous $CD44^{lo}$ naïve CD8 T cells. Cytokine production is shown following a 5 hour stimulation with GP33 peptide in the presence of Brefeldin A. Number represents MFI of respective marker. Bar graphs in (C) and (D) display mean and SEM, compared using paired t-test. Data are representative of 2 to 4 independent experiments with n=2 to 3 mice per group.

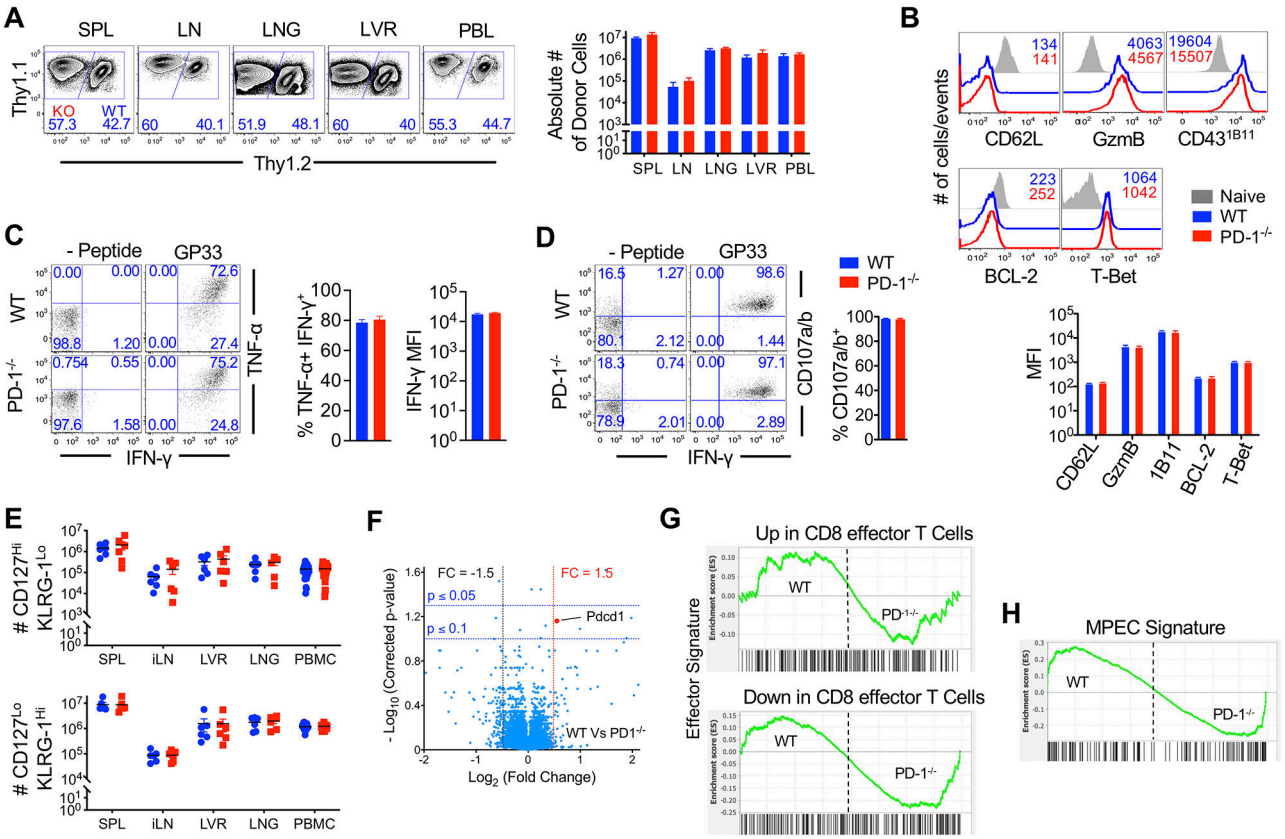

Figure 2. PD-1 signaling in CD8 T cells does not substantially regulate effector programming and peak expansion during acute infection.

Equal numbers ($5x10^4$ cells) of WT (Thy1.2$^+$) and PD-1$^{-/-}$ (Thy1.1$^+$) P14 CD8 T cells were adoptively co-transferred at into naive C57BL/6 mice. Mice were infected with $LCMV_{Arm}$ and analyzed at day 7 post-infection. **(A)** Flow cytometry plots are gated on total donors and show relative WT and PD-1$^{-/-}$ donor antigen-specific CD8 T cell frequencies in spleen (SPL), inguinal lymph node (LN), lung (LNG), liver (LVR), and blood (PBL) at day 7 post-infection. Bar graphs enumerate WT and PD-1$^{-/-}$ donor antigen-specific CD8 T cell numbers in indicated tissues (PBL; number of cells per 10^7 PBMCs) at day 7 post-infection. **(B)** Histograms are gated on WT (blue) or PD-1$^{-/-}$ (red) antigen-specific CD8 T cells isolated from spleen at day 7 post-infection; grey histograms show endogenous CD44^{lo} naïve CD8 T cells. Number represents MFI of respective markers. Bar graph depicts MFI of indicated markers. **(C and D)** Day 7 splenocytes were stimulated with GP33 peptide ex vivo. Flow cytometry plots are gated on donor antigen specific CD8 T cells and depict intracellular staining of IFN-γ and TNF-α (**C**) or surface CD107a/b (**D**). Bar graphs depict IFN-γ MFI, or percent of TNF-α$^+$ or CD107a/b$^+$ of IFN-γ$^+$ donor CD8 T cells. **E**. Dot plots show absolute numbers of MPEC (CD127^{Hi} KLRG-1^{Lo}) and SLEC (CD127^{Lo} KLRG-1^{Hi}) of donor cells in spleen, iLN, liver, lung, and PBMC at day 7 post-infection, compared using paired t-test. Compiled data from 2 independent repeats with n=3 to 5 mice per group per repeat are presented. **(F)** A volcano plot shows fold change (FC) in gene expression for all 42,101 probes between 3 independent replicates of WT and PD-1 effector CD8 T cells with respect to p values depicting significance of change. **G and H**. GSEA of effector **(G) or**

MPEC **(H)** gene signatures in WT and PD-$1^{-/-}$ CD8 T cells. Bar graphs display mean and SEM, compared using paired t-test. Phenotypic data (A to E) are representative of 2 to 5 independent experiments with n=2 to 3 mice per group.

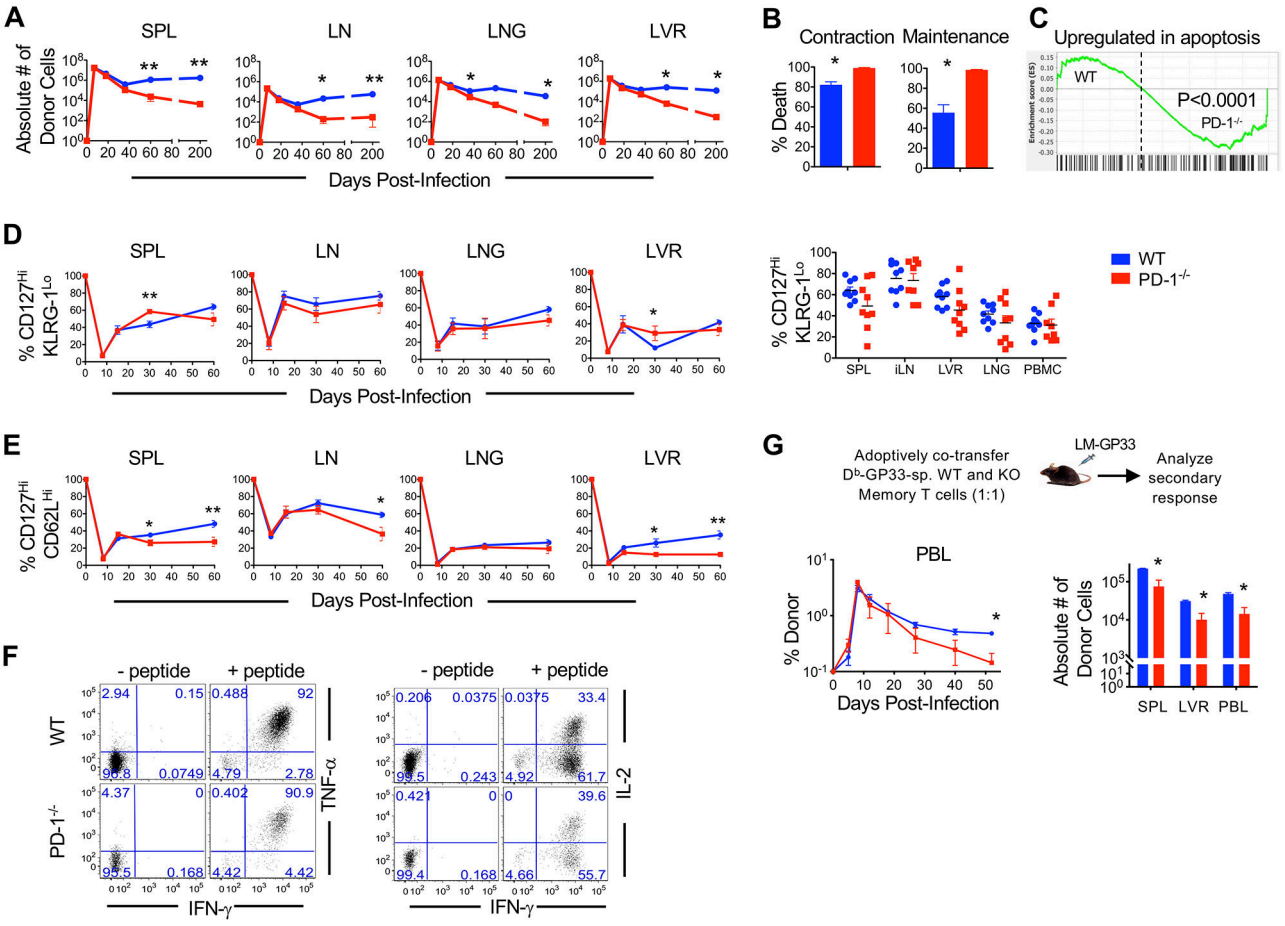

Figure 3. Absence of PD-1 signals in CD8 T cells is associated with increased attrition following antigen clearance.

Equal numbers of WT and PD-1$^{-/-}$ P14 CD8 T cells were adoptively co-transferred at high dose (5x10^4 cells) into C57BL/6 mice. Mice were infected with LCMV$_{Arm}$ and analyzed following infection. **(A).** Antigen-specific WT and PD-1$^{-/-}$ donor CD8 T cell were enumerated longitudinally in spleen (SPL), lymph node (LN), lung (LNG), and liver (LVR). **(B)** Bar graphs depict percent death of WT and PD-1$^{-/-}$ donor CD8 T cells in blood during contraction (day 8-22) and maintenance (day 22-200). **(C).** GSEA analysis shows enrichment of an apoptosis gene signature in day 8 PD-1$^{-/-}$ effector CD8 T cells compared to WT. **(D and E)** Antigen specific WT and PD-1$^{-/-}$ donor CD8 T cells were analyzed longitudinally for expression of CD127^{Hi} KLRG-1^{Lo} memory-fated **(D)** and CD127^{Hi} CD62L^{Hi} T$_{CM}$ subsets **(E)** in the indicated tissues. Dot plots show CD127^{Hi} KLRG-1^{Lo} percentages of donors in the respective compartments at day 60 post-infection. Compiled data from two independent repeats with n=3 to 5 mice per group per repeat are presented. **(F)** Splenocytes were stimulated with GP33 peptide at memory (day 36 post-infection) and donor CD8 T cells were gated. Flow cytometry plots show TNF-α or IL-2 and IFN-γ production by WT and PD-1$^{-/-}$ CD8 T cells. **(G)** WT and PD-1$^{-/-}$ memory CD8 T cells were isolated from splenocytes at day 22 post-infection, and equal numbers were transferred into naïve C57BL/6 recipients at 10^4 cells per mouse. Mice received a heterologous challenge with LM-GP33. The line graph depicts kinetics of donor CD8 T

cells in PBMCs of infected mice. Bar graphs show number of donors in respective tissues at day 52 post-infection. Bar graphs display mean and SEM. Data are representative of 2 to 3 independent experiments with n=3 to 5 mice per group. Paired t-test was used with statistical significance in difference of means represented as *P ≤ 0.05, **P ≤ 0.01.

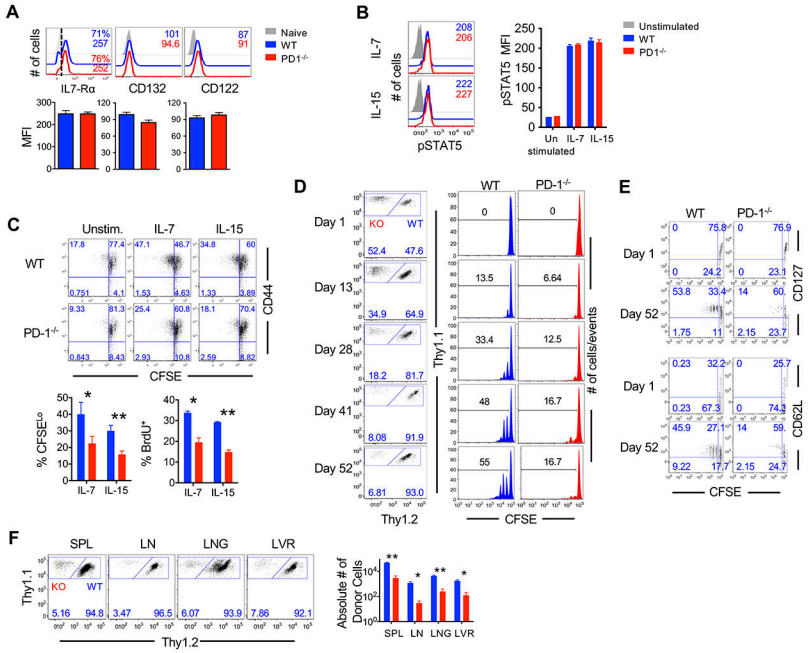

Figure 4. CD8 T cell-specific PD-1 signals are important for memory CD8 T cells capable of homeostatic turnover and maintenance.

(A) WT and PD-1$^{-/-}$ donor CD8 T cells were gated at day 46 post-infection in spleens of infected mice. Histograms show phenotypic markers on WT (blue), PD-1$^{-/-}$ (red) or naïve (grey, filled) CD8 T cells. Numbers in histogram represent MFI. Bar graphs show MFI of IL-7Rα, CD132 and CD122. **(B)** At day 20 post-infection WT and PD-1$^{-/-}$ donor splenocytes were stimulated with IL-7 or IL-15 for 30 minutes and then stained for STAT5 phosphorylation. Histograms show abundance of pSTAT5 in WT (blue), PD-1$^{-/-}$ (red), and unstimulated (grey, filled) CD8 T cells. Bar graphs show MFI of pSTAT5. **(C)** Donor memory WT and PD-1$^{-/-}$ CD8 T cells were isolated at day 30 post-infection and labeled with CFSE and stimulated in vitro with IL-7 and IL-15 for 60 hours. A pulse of BrdU was given for the last 6 hours prior to harvest and flow cytometry analysis. Flow cytometry plots show CFSE dilution of WT and PD-1$^{-/-}$ antigen specific CD8 T cells. Bar graphs depict percent cells that had divided >1 round (CFSE^{Lo}) or incorporated BrdU (BrdU^{+}). **(D to F)** Memory WT (Thy1.2^{+}) and PD-1$^{-/-}$ (Thy1.2^{-}) CD8 T cells were isolated from day 22 post-infection splenocytes and labeled with CFSE and cotransferred into antigen free, C57BL/6 recipients. Donor CD8 T cells were analyzed for homeostatic proliferation of WT and PD-1$^{-/-}$ antigen-specific CD8 T cells at indicated times after adoptive transfer. **(D)** Flow cytometry plots show relative frequencies of WT and PD-1$^{-/-}$ donors. Histograms illustrate CFSE dilution. Number represents percent of cells that have divided at least one time. **(E)** Flow cytometry plots are gated on donor CD8 T cells in day 1 PBMC or day 52 post-transfer splenocytes, and depict CFSE dilution with respect to CD127 and CD62L expression. **(F)** Flow cytometry plots are gated on donor CD8 T cells and depict relative frequency of WT and PD-1$^{-/-}$ donor CD8 T cells in all tissues at day 52 of homeostatic maintenance. Bar graph depicts total numbers of WT and PD-1$^{-/-}$ donor CD8 T cells in spleen, lymph node, lung and liver. Bar graphs display mean and SEM, compared using unpaired (A and B) or paired (C and F) t-tests. Data are representative of two independent experiments with

n=2 to 5 mice per experimental group. Statistical significance in difference of means are represented as *P ≤ 0.05, **P ≤ 0.01.

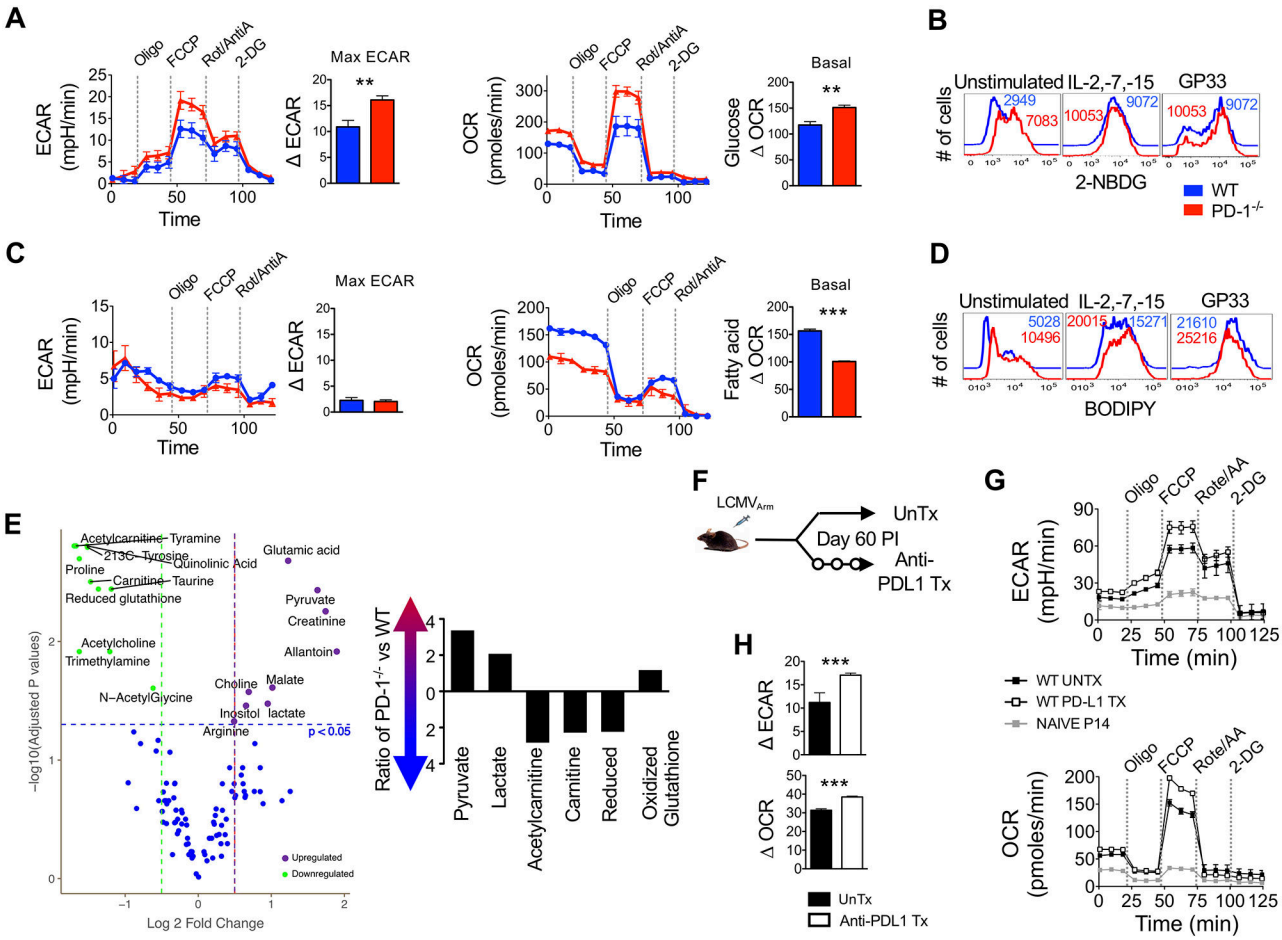

Figure 5. PD-1 signals drive a metabolic switch in CD8 T cells for maintenance of a quiescent memory phenotype.

Equal numbers of WT P14 and PD-$1^{-/-}$ P14 antigen-specific CD8 T cells were adoptively transferred ($5x10^4$ cells) into C57BL/6 mice and mice were infected with $LCMV_{Arm}$. At day 60 post-infection memory donor cells were purified and T cell metabolism was analyzed. **(A)** Metabolic analysis was performed on WT and PD-$1^{-/-}$ donor CD8 T cells in the presence of 10mM glucose with indicated additions of oliomycin (oligo), Trifluoromethoxy carbonylcyanide phenylhydrazone (FCCP), Rotenone and antimycin A (Rot/AntiA) and 2-deoxyglucose (2DG). Line graphs show extracellular acidification (ECAR) and oxygen consumption (OCR) rates over time. Bar graphs depict maximum ECAR and basal OCR values. **(B)** Memory CD8 T cells were incubated with common γ-chain cytokines or unlabeled H-$2D^b$:GP33 tetramer for 36 hours and then glucose uptake (2-NBDG) was analyzed. Representative histograms show WT (blue) or PD-$1^{-/-}$ (red) donor cells. Numbers represent MFI. **(C)** Metabolic analysis was performed on WT and PD-$1^{-/-}$ donor CD8 T cells in the presence of bovine serum albumin (BSA) linked fatty acids. Line graphs show ECAR and OCR values over time. Bar graphs depict maximum ECAR and basal OCR values. **(D)** Memory CD8 T cells were incubated with common γ-chain cytokines or unlabeled H-$2D^b$:GP33 tetramer for 36 hours and then fatty acid (BODIPY) content was analyzed. Representative histograms show WT (blue) or PD-$1^{-/-}$ (red) donor cells.

Numbers represent MFI. **(E)** A volcano plot shows fold change in metabolite values for 110 tested metabolite concentrations in purified WT and PD-$1^{-/-}$ memory CD8 T cells with respect to p-values depicting significance of change. Significantly different metabolites are highlighted. Bar graph shows selected metabolite ratios between PD-$1^{-/-}$ and WT memory CD8 T cells. **(F)** WT P14 CD8 T cells were transferred (10^5 cells) into naïve C57BL/6 mice, which were subsequently infected with $LCMV_{Arm}$. Mice were untreated (UnTx) or treated with anti-PD-L1 following day 60 post-infection for two weeks. **(G)** An XF Seahorse analysis was performed on UnTx and anti-PD-L1 Tx donor memory CD8 T cells in the presence of 10mM glucose. Line graphs show ECAR and OCR. **(H)** Bar graphs show maximum ECAR and basal OCR. Paired (A and C) and unpaired (H) Student's t-tests were used with statistical significance in difference of means represented as $^{**}P \leq 0.01$, $^{***}P \leq 0.001$. Experiments are representative of 2 to 3 experiments with n=3 to 5 mice per group.

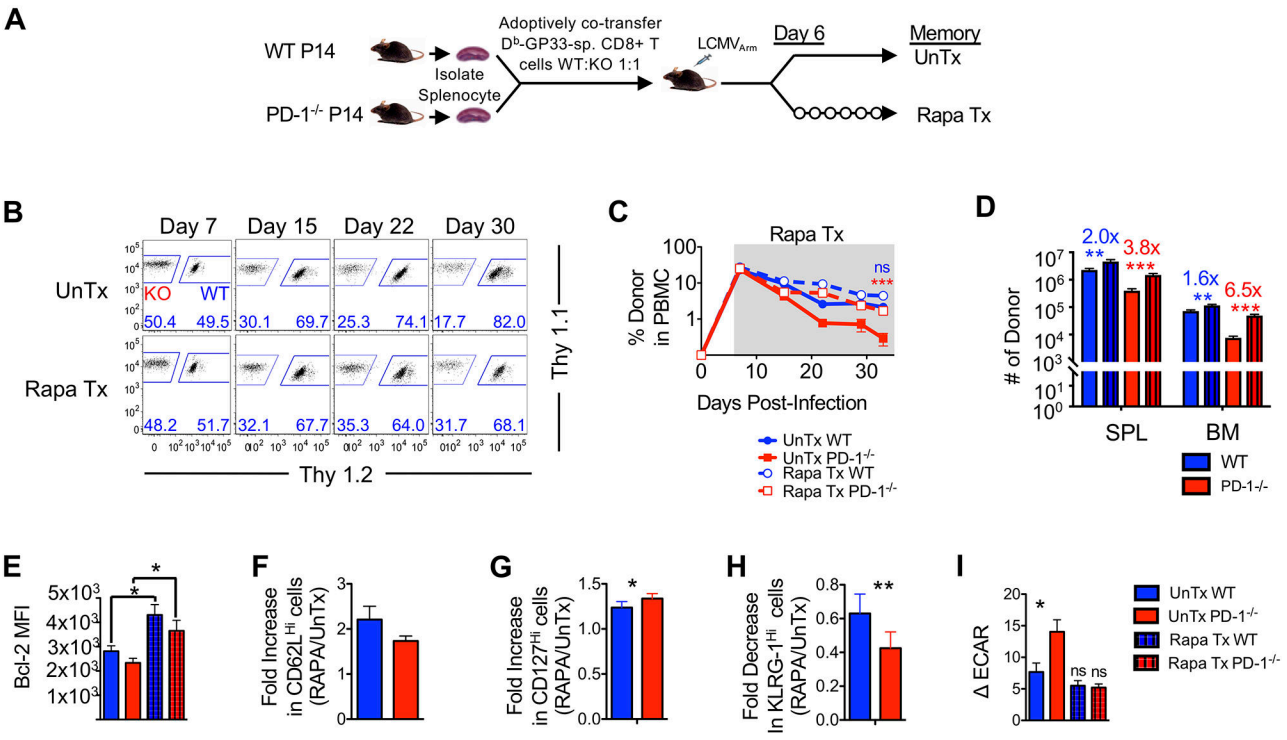

Figure 6. Rapamycin treatment after infection rescues memory attrition in the absence of PD-1 signals.

(A) Equal numbers of WT and PD-1$^{-/-}$ P14 CD8 T cells were adoptively co-transferred ($5x10^4$) into C57BL/6 mice. Mice were infected with $LCMV_{Arm}$ and remained untreated or were treated with Rapamycin (Rapa) daily starting at day 6 post-infection. **(B)** Flow cytometry plots are gated on donor CD8 T cells and show frequencies of WT and PD-1$^{-/-}$ donors in PBMCs. **(C)** Line graph depicts frequency of donors in PBMC during rapamycin treatment. **(D)** Bar graphs show number of donor cells in spleen (SPL) and bone marrow (BM) at day 33 post-infection. Numbers above bar graphs represent fold-change of rapamycin treated by untreated WT (blue) and PD-1$^{-/-}$ (red) respectively day 33 post-infection. **(E)** Bar graph shows MFI of Bcl-2 at day 33 post-infection on gated donor cells. **(F to H)** Bar graph depicts fold-increase in CD62L^{Hi} **(F)** and CD127^{Hi} **(G)** and decrease in KLRG-1^{Hi} **(H)** donor CD8 T cells in spleens from rapamycin-treated animals at day 33 post-infection relative to untreated controls. **(I)** An XF Seahorse analysis was performed on untreated and rapamycin-treated donor CD8 T cells in the presence of 10mM glucose. Bar graph shows basal ECAR in donor cells. Paired (E, F, and G) and unpaired (B, C, D, and G) Student's t-test was used with statistical significance in difference of means represented as *P ≤ 0.05, **P ≤ 0.01, ***P ≤ 0.001. ns, not significant. Data are representative of 2 experiments with n=3 to 5 mice per group.

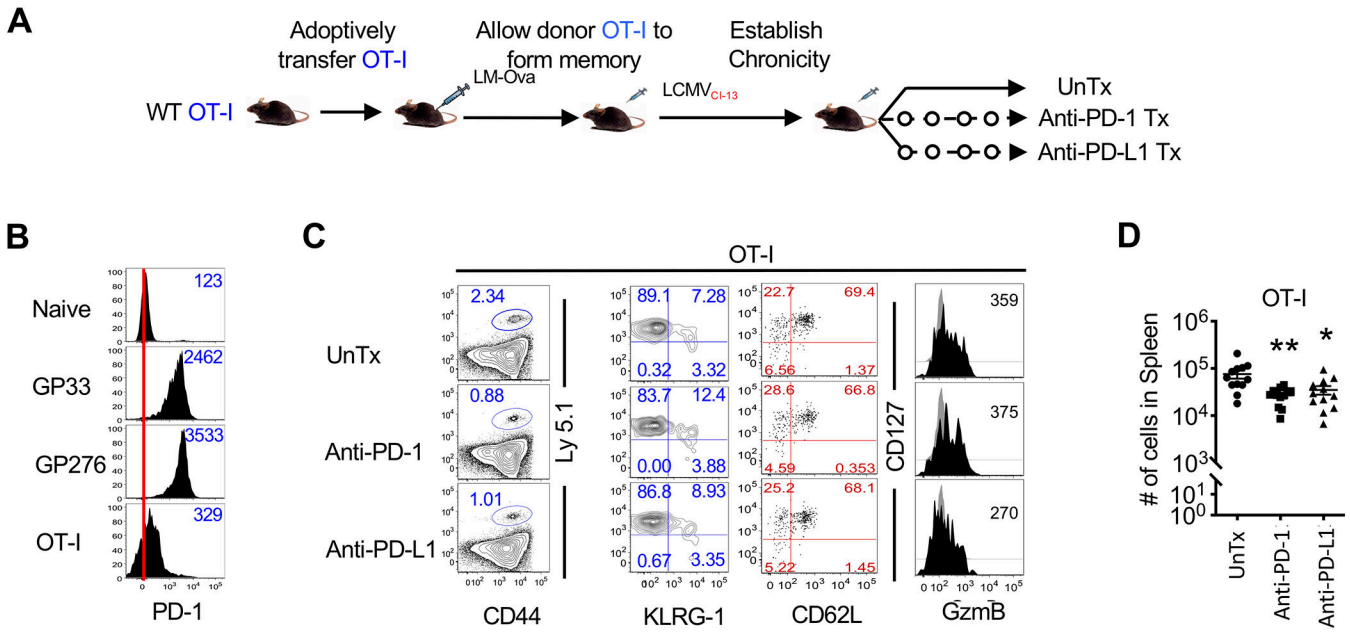

Figure 7. PD-1 checkpoint blockade during chronic infection decreases the total number of antigen-specific memory CD8 T cells.

(A) Naïve, Ly5.1^{+} OT-I CD8 T cells were transferred (10^4 cells) into naïve C57BL/6 mice and infected with LM-OVA. Mice containing memory OT-I CD8 T cells at day 60-75 post-infection were then infected with $LCMV_{CL-13}$ to establish a chronic infection. Chronically infected mice were treated with PBS, anti-PD-1, or anti-PD-L1 starting at day 23 post-infection. **(B)** PBMCs were isolated and characterized at day 22 post-$LCMV_{CL-13}$ infection, prior to initiation of anti-PD-1 or anti-PD-L1 treatment. Histograms show PD-1 expression in naïve (CD44^{Lo}) CD8 T cells, LCMV specific H-2D^{b}:GP33 or H-2D^{b}:GP276 CD8 T cells, and memory OT-I-specific CD8 T cells. Numbers in histogram represent MFI of PD-1. Red line indicates median PD-1 expression in naïve cells. **(C)** Flow cytometry plots show frequency of donor CD8 T cells in spleen upon completion of anti-PD-1 or anti-PD-L1 treatment. Flow cytometry plots are then further gated on donor cells (Ly5.1^{+}) and KLRG-1, CD127, CD62L, and GzmB expression are shown. **(D)** The dot plot shows enumeration of memory OT-I CD8 T cells in spleen at day 39 post-infection. Bar graphs display mean and SEM. Data are representative of three independent experiments with n=4 to 5 mice per group. Unpaired Student's t-test was used with statistical significance in difference of means represented as *P ≤ 0.05), **P ≤ 0.01.